Bartenschlager, R., Lohmann, V., 2000. Replication of hepatitis C virus. J. Gen. Virol. 81, 1631–1648.
Bernardi, P., 1999. Mitochondrial transport of cations: channels, exchangers, and permeability transition. Physiol. Rev. 79, 1127–1155.
Bonkovsky, H.L., Banner, B.F., Rothman, A.L., 1997. Iron and chronic viral hepatitis. Hepatology 25, 759–768.
Bukh, J., Miller, R.H., Purcell, R.H., 1995. Genetic heterogeneity of hepatitis C virus: quasispecies and genotypes. Semin. Liver Dis. 15, 41–63.
Choi, J., Ou, J.H., 2006. Mechanisms of liver injury. III. Oxidative stress in the pathogenesis of hepatitis C virus. Am. J. Physiol. Gastrointest. Liver Physiol. 290, G847–G851.
Farinati, F., Cardin, R., De Maria, N., Della Libera, G., Marafin, C., Lecis, E., et al., 1995. Iron storage, lipid peroxidation and glutathione turnover in chronic anti-HCV positive hepatitis. J. Hepatol. 22, 449–456.
Hayashi, H., Takikawa, T., Nishimura, N., Yano, M., Isomura, T., Sakamoto, N., 1994. Improvement of serum aminotransferase levels after phlebotomy in patients with chronic active hepatitis C and excess hepatic iron. Am. J. Gastroenterol. 89, 986–988.
Ikeda, K., Saitoh, S., Suzuki, Y., Kobayashi, M., Tsubota, A., Koida, I., et al., 1998. Disease progression and hepatocellular carcinogenesis in patients with chronic viral hepatitis: a prospective observation of 2215 patients. J. Hepatol. 28, 930–938.
Kageyama, F., Kobayashi, Y., Murohisa, G., Shimizu, E., Suzuki, F., Kikuyama, M., et al., 1998. Failure to respond to interferon-alpha 2a therapy is associated with increased hepatic iron levels in patients with chronic hepatitis C. Biol. Trace Elem. Res. 64, 185–196.
Kato, J., Kobune, M., Nakamura, T., Kuroiwa, G., Takada, K., Takimoto, R., et al., 2001. Normalization of elevated hepatic 8-hydroxy-2′-deoxyguanosine levels in chronic hepatitis C patients by phlebotomy and low iron diet. Cancer Res. 61, 8697–8702.
Kato, J., Miyanishi, K., Kobune, M., Nakamura, T., Takada, K., Takimoto, R., et al., 2007. Long-term phlebotomy with low-iron diet therapy lowers risk of development of hepatocellular carcinoma from chronic hepatitis C. J. Gastroenterol. 42, 830–836.
Korenaga, M., Wang, T., Li, Y., Showalter, L.A., Chan, T., Sun, J., et al., 2005. Hepatitis C virus core protein inhibits mitochondrial electron transport and increases reactive oxygen species (ROS) production. J. Biol. Chem. 280, 37481–37488.
Kowdley, K.V., 2004. Iron, hemochromatosis, and hepatocellular carcinoma. Gastroenterology 127, S79–S86.
Lau, J.Y., Xie, X., Lai, M.M., Wu, P.C., 1998. Apoptosis and viral hepatitis. Semin. Liver Dis. 18, 169–176.
Li, Y., Boehning, D.F., Qian, T., Popov, V.L., Weinman, S.A., 2007. Hepatitis C virus core protein increases mitochondrial ROS production by stimulation of Ca^{2+} uniporter activity. FASEB J. 21, 2474–2485.
Maeda, T., Miyazono, Y., Ito, K., Hamada, K., Sekine, S., Horie, T., 2010. Oxidative stress and enhanced paracellular permeability in the small intestine of methotrexate-treated rats. Cancer Chemother. Pharmacol. 65, 1117–1123.
Masubuchi, Y., Nakayama, S., Horie, T., 2002. Role of mitochondrial permeability transition in diclofenac-induced hepatocyte injury in rats. Hepatology 35, 544–551.
Moriya, K., Nakagawa, K., Santa, T., Shintani, Y., Fujie, H., Miyoshi, H., et al., 2001. Oxidative stress in the absence of inflammation in a mouse model for hepatitis C virus-associated hepatocarcinogenesis. Cancer Res. 61, 4365–4370.
Moriya, K., Miyoshi, H., Shinzawa, S., Tsutsumi, T., Fujie, H., Goto, K., et al., 2010. Hepatitis C virus core protein compromises iron-induced activation of antioxidants in mice and HepG2 cells. J. Med. Virol. 82, 776–792.
Muckenthaler, M.U., 2008. Fine tuning of hepcidin expression by positive and negative regulators. Cell Metab. 8, 1–3.
Nishioka, K., Watanabe, J., Furuta, S., Tanaka, E., Iino, S., Suzuki, H., et al., 1991. A high prevalence of antibody to the hepatitis C virus in patients with hepatocellular carcinoma in Japan. Cancer 67, 429–433.
Oberley, T.D., 2002. Oxidative damage and cancer. Am. J. Pathol. 160, 403–408.
Okuda, M., Li, K., Beard, M.R., Showalter, L.A., Scholle, F., Lemon, S.M., et al., 2002. Mitochondrial injury, oxidative stress, and antioxidant gene expression are induced by hepatitis C virus core protein. Gastroenterology 122, 366–375.
Olynyk, J.K., Reddy, K.R., Di Bisceglie, A.M., Jeffers, L.J., Parker, T.I., Radick, J.L., et al., 1995. Hepatic iron concentration as a predictor of response to interferon alfa therapy in chronic hepatitis C. Gastroenterology 108, 1104–1109.
Otani, K., Korenaga, M., Beard, M.R., Li, K., Qian, T., Showalter, L.A., et al., 2005. Hepatitis C virus core protein, cytochrome P450 2E1, and alcohol produce combined mitochondrial injury and cytotoxicity in hepatoma cells. Gastroenterology 128, 96–107.
Park, J.S., Yang, J.M., Min, M.K., 2000. Hepatitis C virus nonstructural protein NS4B transforms NIH3T3 cells in cooperation with the Ha-ras oncogene. Biochem. Biophys. Res. Commun. 267, 581–587.
Raffaello, A., De Stefani, D., Rizzuto, R., 2012. The mitochondrial Ca^{2+} uniporter. Cell Calcium 52, 16–21.
Ray, R.B., Meyer, K., Ray, R., 2000. Hepatitis C virus core protein promotes immortalization of primary human hepatocytes. Virology 271, 197–204.
Silva, I.S., Perez, R.M., Oliveira, P.V., Cantagalo, M.I., Dantas, E., Sisti, C., et al., 2005. Iron overload in patients with chronic hepatitis C virus infection: clinical and histological study. J. Gastroenterol. Hepatol. 20, 243–248.
Walters, G.O., Miller, F.M., Worwood, M., 1973. Serum ferritin concentration and iron stores in normal subjects. J. Clin. Pathol. 26, 770–772.
Wang, T., Weinman, S.A., 2006. Causes and consequences of mitochondrial reactive oxygen species generation in hepatitis C. J. Gastroenterol. Hepatol. 21 (Suppl. 3), S34–S37.
Wang, T., Campbell, R.V., Yi, M.K., Lemon, S.M., Weinman, S.A., 2010. Role of hepatitis C virus core protein in viral-induced mitochondrial dysfunction. J. Viral Hepat. 17, 784–793.

Hepatology Research

Hepatology Research 2014; 44: E240–E252 doi: 10.1111/hepr.12275

Original Article

Effect of the infectious dose and the presence of hepatitis C virus core gene on mouse intrahepatic CD8 T cells

Yutaka Horiuchi,[1] Akira Takagi,[1] Nobuharu Kobayashi,[1] Osamu Moriya,[1] Toshinori Nagai,[2] Kyoji Moriya,[3] Takeya Tsutsumi,[3] Kazuhiro Koike[3] and Toshitaka Akatsuka[1]

Departments of [1]Microbiology and [2]Pathology, Saitama Medical University, Saitama, and [3]Department of Gastroenterology, Graduate School of Medicine, The University of Tokyo, Tokyo, Japan

Aim: Chronic hepatitis C viral (HCV) infections often result in ineffective CD8 T-cell responses due to functional exhaustion of HCV-specific T cells. However, how persisting HCV impacts CD8 T-cell effector functions remains largely unknown. The aim of this study is to examine the effect of the infectious dose and the presence of HCV core gene.

Methods: We compared responses of intrahepatic CD8 T cells during infection of wild-type or HCV core transgenic (Tg) mice with various infectious doses of HCV-NS3-expressing recombinant adenovirus (Ad-HCV-NS3).

Results: Using major histocompatibility complex class I tetramer and intracellular interferon (IFN)-γ staining method to track HCV-NS3-specific CD8 T cells, we found that a significant expansion of HCV-NS3-specific CD8 T cells was restricted to a very narrow dosage range. IFN-γ production by intrahepatic CD8 T cells in HCV core Tg mice was suppressed as compared with wild-type mice. Higher levels of expression of regulatory molecules, Tim-3 and PD-1, by intrahepatic CD8 T cells and PD-L1 by intrahepatic antigen-presenting cells were observed in HCV core Tg mice following Ad-HCV-NS3 infection, and the expression increased dependent on infectious dose. Furthermore, we found a significant inverse correlation between the percentages of IFN-γ-producing cells and expression of regulatory molecules in antigen-specific intrahepatic CD8 T cells.

Conclusion: High infectious dose and the presence of HCV core gene were strongly involved in ineffective CD8 T-cell responses. We consider that HCV core Tg mouse infected with high infectious dose of Ad-HCV-NS3 is useful as a chronic infection model in the development of immunotherapy for chronic hepatitis C.

Key words: core, functional exhaustion, hepatitis C, infectious dose, T cell

INTRODUCTION

HEPATITIS C VIRUS (HCV) is a positive-sense single-stranded RNA virus of the genus *Hepacivirus* in the family *Flaviviridae*, and it infects 170 million people worldwide.[1] Approximately 10–60% of the patients clear HCV spontaneously during the acute phase of infection,[2] while the others develop chronic persistent HCV infection that eventually leads to liver cirrhosis and hepatocellular carcinoma.[3] HCV-specific cytotoxic T lymphocytes (CTL) play a major role in viral control during acute infection.[4] Nevertheless, during persistent infection, HCV-specific CTL effector functions are significantly impaired.

T-cell exhaustion is one of the remarkable features of chronic HCV infection. In chronically HCV-infected individuals, the frequencies of CTL are relatively low; similarly, the proliferative capacity as well as effector functions of HCV-specific T cells are impaired, and the production of type I cytokines (i.e. interleukin-2 and interferon [IFN]-γ) is dramatically suppressed.[5–8]

It appears that the major factors which determine duration and magnitude of an antiviral immune response are antigen (Ag) localization, dose and kinetics.[9] For example, high doses of widely disseminating strains of lymphocytic choriomeningitis virus (LCMV) exhaust antiviral CTL leading to establishment of a persistent infection.[10] Physical deletion of anti-LCMV CTL is most likely preceded by their functional impairment with the inability to produce effector cytokines.[11,12]

Correspondence: Professor Toshitaka Akatsuka, Department of Microbiology, Faculty of Medicine, Saitama Medical University, 38 Morohongo, Moroyama-cho, Iruma-gun, Saitama 350-0495, Japan. Email: akatsuka@saitama-med.ac.jp
Received 21 May 2013; revision 8 November 2013; accepted 11 November 2013.

Moreover, Wherry *et al.* showed that not only the persistence of a viral Ag, but also the initial Ag level is an important factor determining the quality of the antiviral memory response.[13]

Hepatitis C virus core protein has been reported to suppress T-cell response. HCV core-mediated inhibition of T-cell response can occur via either modulation of pro-inflammatory cytokine production by antigen-presenting cells (APC; i.e. monocyte and dendritic cells)[14] or direct effect on T cells.[15–17] Because the liver is the major site of HCV infection, it is crucial to understand the regulation of host immunity by HCV core in the liver compartment and the impact of HCV core-induced immune dysregulation in facilitating HCV persistence.

Hepatitis C virus does not infect small laboratory animals. The lack of a small animal model has hampered studies attempting to elucidate the mechanism of HCV-mediated suppression of antiviral CD8 T-cell activity and caused difficulty in the development of a therapeutic and/or prophylactic HCV vaccine.

Adenoviral vectors efficiently and reproducibly transfer foreign DNA into the livers of immunocompetent experimental animals. i.v. administration of adenoviral vectors of more than 10^9 infectious units/mouse results in infection and Ag expression in more than 90% of hepatocytes and acute self-limiting viral hepatitis.[18,19]

In this study, to develop a useful animal model in the development of immunotherapy for chronic hepatitis C, we examined the responses of intrahepatic CD8 T cells of HCV core transgenic (Tg) mice with various infectious doses of HCV-NS3-recombinant adenovirus (Ad-HCV-NS3).

METHODS

Mice

C57BL/6 MICE WERE purchased from Clea Japan (Tokyo, Japan), and Tokyo Laboratory Animal Science (Tokyo, Japan). Production of HCV core Tg mice has been described.[20] The core gene of HCV placed downstream of a transcriptional regulatory region from hepatitis B virus, which has been shown to allow an expression of genes in Tg mice without interfering with mouse development,[21] was introduced into C57BL/6 mouse embryos (Clea Japan). Eight- to 10-week-old mice were used for all experiments. The mice were housed in appropriate animal care facilities at Saitama Medical University (Saitama, Japan) and were handled according to international guidelines. The experimental protocols were approved by the Animal Research Committee of Saitama Medical University (#855).

HCV-NS3 recombinant adenovirus

Adenovirus HCV-NS3 expressing the fusion protein, comprising the entire HCV-NS3 and 3X flag, was constructed by using the AdEasy XL adenoviral vector system (Agilent Technologies, Santa Clara, CA, USA). The HCV-NS3 gene corresponding to amino acid residues 1027–1657 was amplified from the plasmid pBRTM/HCV1-3011con which contains the entire DNA sequence derived from the HCV H77 clone (kindly provided by Charls M. Rice, The Rockefeller University, New York, NY, USA)[22] by polymerase chain reaction. The recombinant Ad-HCV-NS3 vector was linearized by PacI digestion, and then transfected into 293 cells using Lipofectamine LTX (Invitrogen, Carlsbad, CA, USA) to generate adenovirus. Ad-HCV-NS3 expressing transgene NS3 was amplified in 293 cells, purified by a series of cesium chloride ultracentrifugation gradients and stored at −80°C until use. Mice were injected i.v. with 2×10^7, 1×10^9 and 1×10^{10} plaque-forming units (PFU) of Ad-HCV-NS3 or Adψ5 control vector. The experimental protocol regarding construction of recombinant adenovirus and infection of mice was approved by the Recombinant DNA Advisory Committee of Saitama Medical University (#1073).

Isolation of intrahepatic leukocytes

The liver was perfused with phosphate-buffered saline (PBS) plus 0.05% collagenase via the portal vein. Perfused livers were smashed through a 100-μm cell strainer (BD Biosciences, San Jose, CA, USA). The cell suspension was centrifuged with 35% Percoll at 320 *g* for 10 min, and the cell pellet was cultured in a plastic Petri dish in RPMI-1640 medium supplemented with 10% fetal calf serum (FCS; R-10) for 1.5 h to remove adherent cells. Then, non-adherent cells were harvested, washed twice with R-10 and used as intrahepatic lymphocytes (IHL). Adherent cells were used as intrahepatic APC).

Intracellular IFN-γ staining

The IHL were resuspended in R-10. In each well of a 96-well round-bottomed plate, 2×10^6 IHL were incubated for 5 h at 37°C in R-10 containing 50 ng/mL phorbol myristate acetate (PMA; Sigma-Aldrich, St Louis, MI, USA), 1 μM ionophore A23187 (Sigma-Aldrich) and 1 μg/mL brefeldin-A (BD Biosciences). The cells were then washed twice with ice-cold PBS (−) and incubated for 10 min at 4°C with a rat antimouse

CD16/CD32 monoclonal Ab (mAb; Fc Block; BD Biosciences) at a concentration of 1 μg/well. Following incubation, the cells were washed twice with ice-cold PBS (−) and stained with a PE-conjugated HCV-NS3 H-2Db tetramer (Tet-603; GAVQNEVTL; Medical and Biological Laboratories, Nagoya, Japan)[23] and peridinin chlorophyll protein (PerCP)-conjugated rat antimouse CD8 MAb (clone 53-6.7; BD Biosciences) for 30 min at 4°C in staining buffer (PBS with 1% FCS and 0.1% NaN_3). After the cells were washed twice, they were fixed and permeabilized by using a Cytofix/Cytoperm kit (BD Biosciences) and stained with a fluorescein isothiocyanate (FITC)-conjugated rat antimouse IFN-γ mAb (clone XMG1.2; BD Biosciences). After the cells were washed, flow cytometric analyses were performed with a FACScanto II flow cytometer (Becton Dickinson, Franklin Lakes, NJ, USA), and the data were analyzed with FACSdiva software (Becton Dickinson).

PD-1 and Tim-3 staining

Intrahepatic lymphocytes were prepared and treated with an antimouse CD16/CD32 mAb as described above for intracellular IFN-γ staining and then stained with a PE-conjugated HCV-NS3 H-2Db tetramer, PerCP-conjugated anti-CD8a (BD Biosciences), FITC-conjugated anti-PD-1 (eBioscience, San Diego, CA, USA) and Alexa647-conjugated anti-Tim-3 (Biolegend, San Diego, CA, USA) for 30 min at 4°C. After the cells were washed twice, they were fixed with PBS containing 1% formaldehyde and 2% FCS and analyzed by flow cytometry.

PD-L1 staining

Intrahepatic APC were prepared and treated with an antimouse CD16/CD32 mAb as described above for intracellular IFN-γ staining and then stained with a FITC-conjugated anti-CD11c (BD Biosciences) and PE-conjugated anti-PD-L1 (eBioscience) for 30 min at 4°C. After the cells were washed twice, they were fixed with PBS containing 1% formaldehyde and 2% FCS and analyzed by flow cytometry.

HCV core Ag detection

For the detection of HCV core Ag in the liver, liver tissue samples isolated 7 and 14 days post-infection were homogenized in RIPA B buffer (50 mM Tris pH 7.5, 1% NP40, 0.15 M NaCl, 1 mM phenylmethylsulfonyl fluoride) to make 10% (w/v) extract. Liver tissue extracts were assessed using Lumispot Eiken HCV Ag assay kit (Lumispot-Ag; Eiken Chemical, Tokyo, Japan).

Histology and immunohistology staining

Liver tissue samples isolated 7 and 14 days post-infection were used for histological studies. Paraffin sections (4-μm thick) were stained with hematoxylin–eosin safranin O. For immunohistology, 5-μm thick acetone-fixed frozen sections were incubated with rat anti-CD8 (BD Biosciences), followed by biotin-conjugated antirat immunoglobulin G and ABC staining system (Santa Cruz Biotechnology, Santa Cruz, CA, USA).

Persisting HCV-NS3 Ag detection

For the detection of persisting HCV-NS3 Ag in the liver, liver tissue samples isolated 21 days post-infection were homogenized in RIPA C buffer (50 mM Tris pH 7.5, 1% Triton X-100, 300 mM NaCl, 5 mM ethylenediaminetetraacetic acid, 0.02% NaN_3) to make 2% (w/v) extract and used for immune precipitation/western blot assay. Liver tissue extracts were incubated with protein-G sepharose beads for 30 min at 4°C to remove non-specifically bound proteins. After centrifugation, supernatants were incubated with anti-Flag-M2 antibody (Sigma-Aldrich) coupled protein-G sepharose beads for 2 h at 4°C. After centrifugation, HCV-NS3-3xFlag fusion protein bound to the beads were dissolved in sample buffer and separated on 10% sodium dodecylsulfate polyacrylamide gel electrophoresis gels (Mini PROTEAN TGX gel; Bio-Rad, Hercules, CA, USA) for immunoblot analysis using anti-Flag-M2 antibody and goat anti-mouse Ig horseradish peroxidase (KPL, Gaithersburg, MD, USA). Electrochemiluminescence Prime Western Blotting Detection Reagent (GE Healthcare, Little Chalfont, UK) was used for chemiluminescent detection.

Statistical analysis

Mann–Whitney *U*-tests were used to evaluate the significance of the differences. Correlations between parameters were tested for statistical significance by Pearson correlation.

RESULTS

Functional exhaustion of Ag-specific CD8 IHL with high infectious dose and the impaired Ag-specific CD8 IHL responses in core Tg mice

TO DETERMINE THE effect of the amount of virus dose, we evaluated hepatic inflammation and compared the magnitude of HCV-NS3-specific CD8

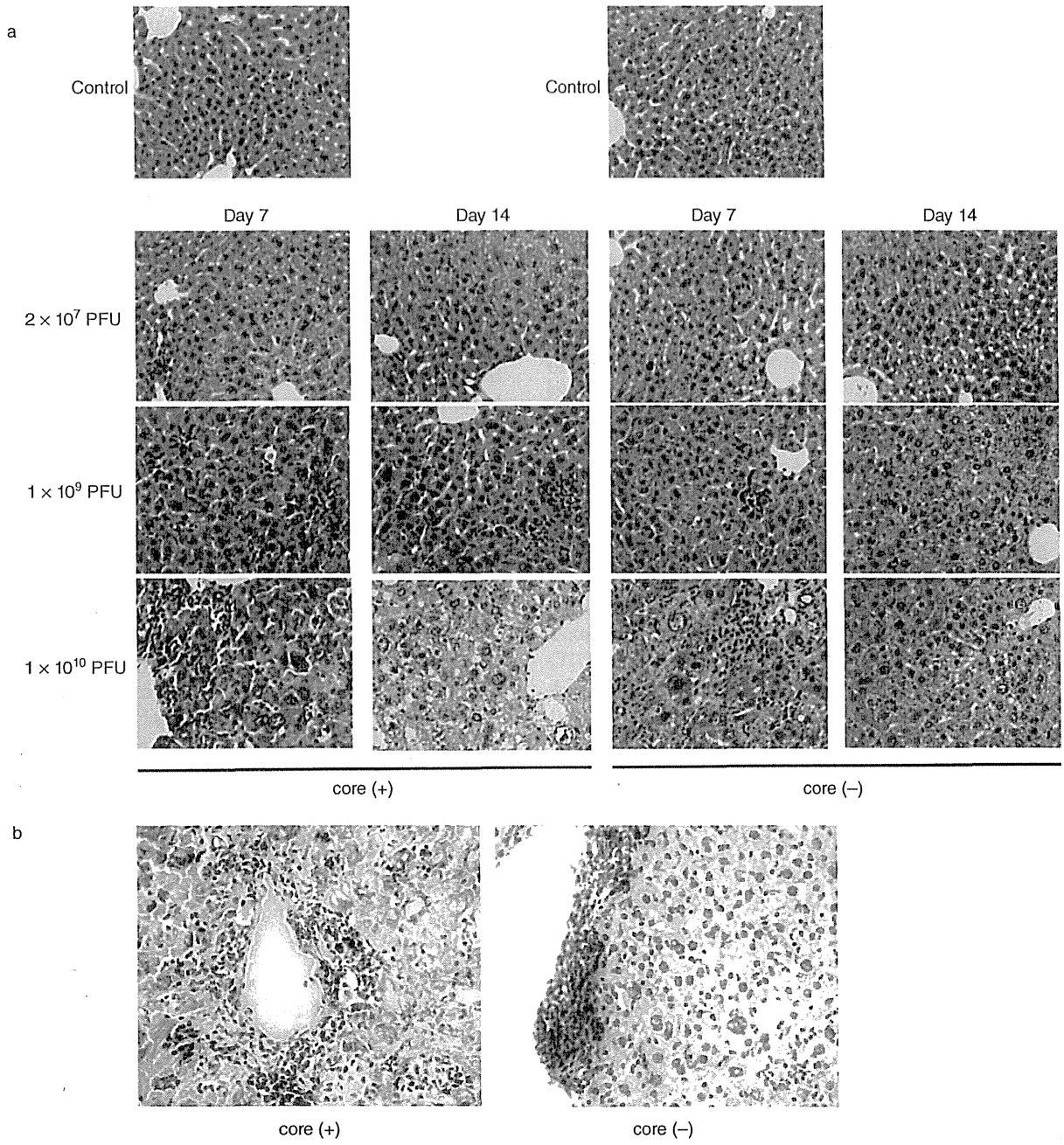

Figure 1 Adenovirus (Ad) infection-mediated hepatic inflammation in mouse liver. Hepatitis C virus (HCV) core (+) and core (–) mice were infected with 2×10^7, 1×10^9 and 1×10^{10} plaque-forming units (PFU) of Ad-HCV-NS3 i.v. and analyzed at 7 and 14 days post-infection. (a) Harvested liver tissues were analyzed by hematoxylin–eosin staining for assessment of hepatic inflammation. (b) Frozen liver sections were analyzed by CD8 staining. Liver infected with 1×10^{10} PFU and harvested at 7 days post-infection was used (original magnifications: [a] ×100; [b] ×200). (c,d) The frequency and number of hepatic CD8 lymphocytes were assessed by flow cytometric analysis. There were no differences in the frequency and number of hepatic CD8 lymphocytes between core (+) mice and core (–) mice. (e) Detection of HCV core antigen in the liver. Liver tissue extracts were assessed using Lumispot Eiken HCV Ag assay kit. There were no differences in core protein expression between Ad-infected and non-infected livers. ■, day 7; ▨, day 14; □, day 21.

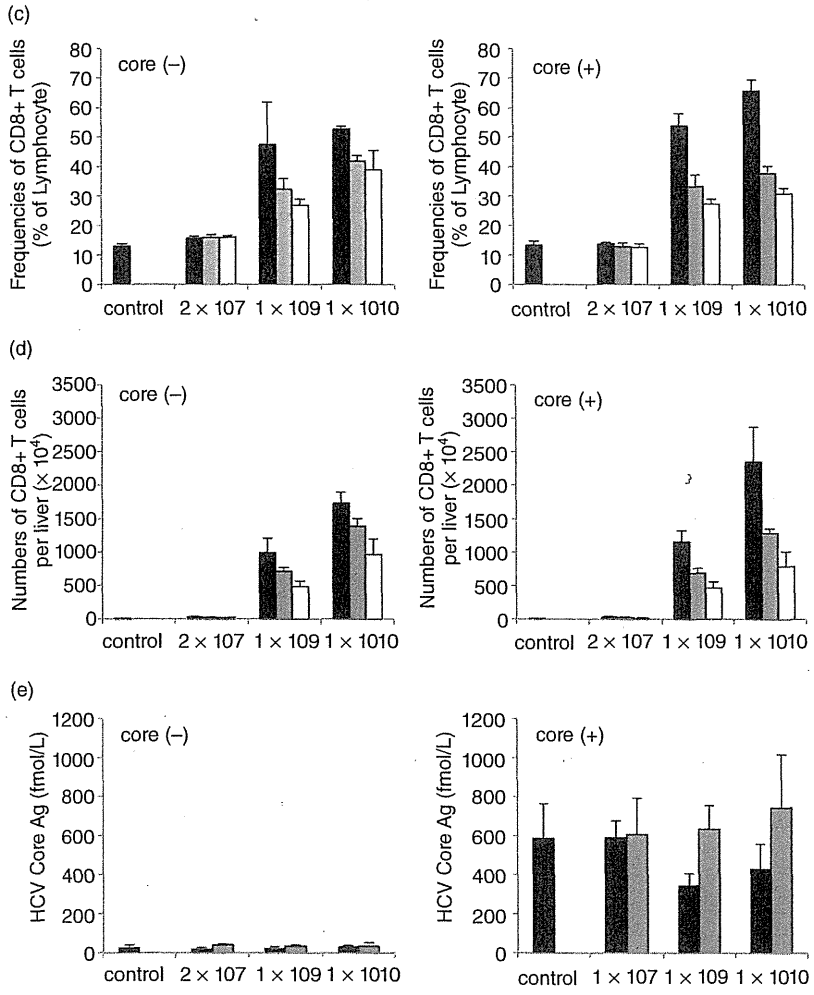

Figure 1 *Continued*

T-cell responses and their effector function in the liver of mice infected with 2×10^7, 1×10^9 and 1×10^{10} PFU Ad-HCV-NS3.

In histological studies, we observed Ad-infection-mediated hepatic inflammation in mice injected with 1×10^9 and 1×10^{10} PFU. Especially, infection with 1×10^{10} PFU caused drastic infiltrations of inflammatory cells (Fig. 1a). We also observed that CD8 lymphocytes infiltrated into the lobular areas of the infected liver in mice injected with 1×10^{10} PFU (Fig. 1b). At 7 days post-infection, we found by flow cytometric assay that the numbers and the frequencies of CD8 T cells in the liver were markedly increased after infection with 1×10^9 PFU and 1×10^{10} PFU, and the increased CD8 T cells decreased with time (Fig. 1c). We did not find significant differences between the number of CD8 T cells of core (+) and core (–) at each time point and infectious dose.

In addition, we evaluated core protein expression in the liver in each infectious dose at 7 and 14 days post-infection; there was no significant difference in core protein expression between Ad-infected and non-infected livers (Fig. 1e).

Using major histocompatibility complex (MHC) class I tetramer complexed with the H2-Db-binding HCV-NS3 GAVQNEVTL epitope, we found that i.v. infection with 2×10^7 PFU generally elicited only a weak expansion of HCV-NS3 tet^+ $CD8^+$ IHL (Fig. 2a,b) and IFN-γ^+ HCV-NS3 tet^+ $CD8^+$ IHL (Fig. 2a,c). In contrast, infection with 1×10^9 PFU induced a significant proliferation

of HCV-NS3 tet$^+$ CD8$^+$ IHL (Fig. 2a,b) and IFN-γ$^+$ HCV-NS3 tet$^+$ CD8$^+$ IHL (Fig. 2a,c).

In each infectious dose, HCV-NS3 tet$^-$ CD8 IHL did not show the diminution of elicited IFN-γ production (Fig. 2a). In contrast, HCV-NS3 tet$^+$ CD8 IHL showed the dose-dependent diminution of elicited IFN-γ production (Fig. 2d). Especially, infection with 1×10^{10} PFU led to a dramatic diminution of the elicited IFN-γ production in HCV-NS3 tet$^+$ CD8$^+$ IHL (Fig. 2a,d). These indicate that high infectious dose of Ad-HCV-NS3 cause NS3 Ag-specific immunosuppression.

As shown in Figure 2(c), the number of IFN-γ-producing HCV-NS3 tetramer$^+$ CD8 T cells in the liver of core (+) mice was lower than that of core (−) mice following PMA/ionophore stimulation. In addition, the percentage of IFN-γ-producing CD8 lymphocytes in tetramer$^+$ CD8 IHL of core (+) mice was suppressed as compared with core (−) mice following PMA/ionophore stimulation (Fig. 2d). These suggest that the presence of HCV core gene significantly impair antiviral effector CD8 T-cell responses in the liver.

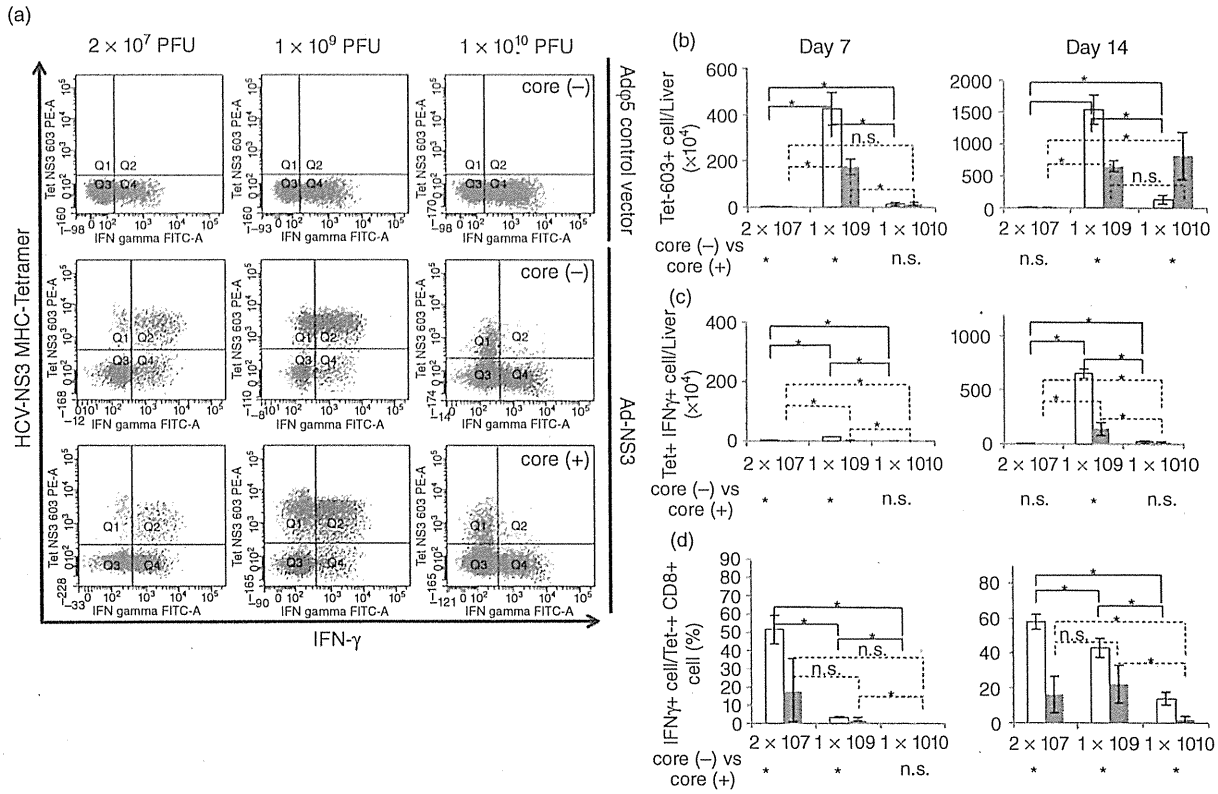

Figure 2 Impaired CD8$^+$ T-cell responses in the livers of high infectious doses. (a) Flow cytometric dot gram gating on the CD8 lymphocyte at day 14 post-infection. Graded doses of adenovirus (Ad)-hepatitis C virus (HCV)-NS3 were administrated i.v and NS3-specific intrahepatic cytotoxic T lymphocytes (CTL) were analyzed using major histocompatibility complex (MHC) class I tetramer and intracellular interferon (IFN)-γ staining method. Data show one representative mouse per group ($n = 3$). (b) The number of MHC tetramer$^+$ CD8 lymphocytes in the liver of core (−) and core (+) mice at day 7 and day 14 following Ad-HCV-NS3 infection (*$P < 0.05$; n.s., not statistically significant). (c) The number of tetramer+ intracellular IFN-γ + CD8 lymphocytes in the liver of core (−) and core (+) mice at day 7 and day 14 following Ad-HCV-NS3 infection. Intrahepatic lymphocytes (IHL) were restimulated with phorbol myristate acetate (PMA)/ionophore for 5 h and IFN-γ production was determined by intracellular cytokine staining (*$P < 0.05$; n.s., not statistically significant). (d) The percentage of intracellular IFN-γ$^+$ CD8 lymphocytes in tetramer$^+$ CD8 IHL of core (−) and core (+) mice on day 7 and day 14 following Ad-HCV-NS3 infection. IHL were restimulated with PMA/ionophore for 5 h and IFN-γ production was determined by intracellular cytokine staining (*$P < 0.05$; n.s., not statistically significant). □, core (−); ■, core (+).

The existence of HCV core gene cause higher expression of suppression molecules

The PD-1 and Tim-3 inhibitory pathways have been reported to play important roles in the dysfunction of effector T-cell response during viral infection. For instance, the expression of PD-1 is increased on functionally exhausted CD8 T cells during chronic viral infection.[15] To investigate the relation between the viral infectious doses or the expression of HCV core gene in the liver and suppression marker expression of antiviral CD8 IHL, we examined the expression for both PD-1 and Tim-3 in the CD8 IHL and PD-L1 in the intrahepatic APC of core (+) and core (–) following various doses Ad-HCV-NS3 infection.

We found that i.v. infection with 1×10^{10} PFU induced a significant expression of PD-1 and Tim-3 by Ad-HCV-NS3 specific intrahepatic CD8 T cells (Fig. 3).

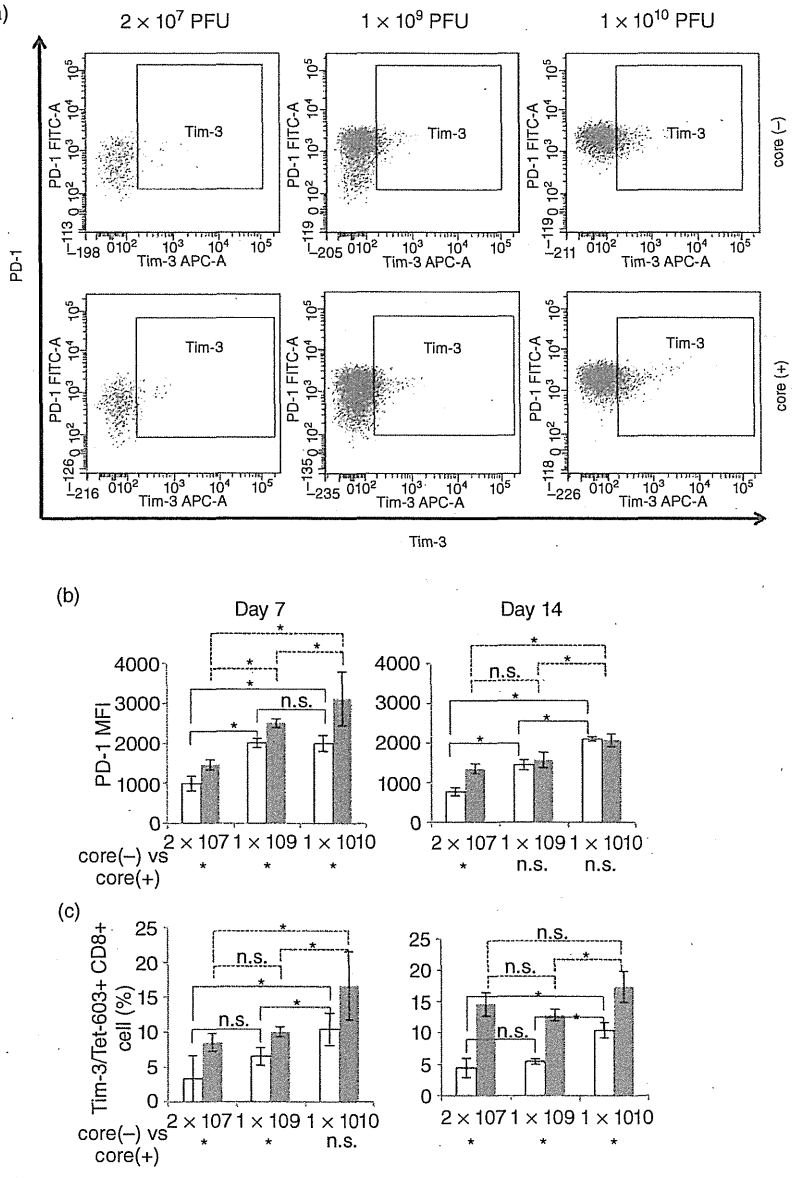

Figure 3 Differential suppression marker expression on NS3-specific CD8 lymphocyte in various infectious doses. (a) Flow cytometric dot gram gating on the hepatitis C virus (HCV)-NS3-tetramer$^+$ CD8 lymphocyte at day 14 post-infection. Graded doses of adenovirus (Ad)-HCV-NS3 were administrated i.v and NS3-specific intrahepatic cytotoxic T lymphocytes (CTL) were analyzed using major histocompatibility complex (MHC) class I tetramer and anti-PD-1 and anti-Tim-3 monoclonal antibody. Data show one representative mouse per group ($n = 3$). (b) The median fluorescence index (MFI) value of PD-1 expressed on HCV-NS3-specific CD8 intrahepatic lymphocytes (IHL) from core (–) and core (+) mice at 14 days following Ad-HCV-NS3 infection. (*$P < 0.05$; n.s., not statistically significant). (c) The number of Tim-3$^+$ HCV-NS3-specific CD8 IHL from core (–) and core (+) mice at 14 days following Ad-HCV-NS3 infection. (*$P < 0.05$; n.s., not statistically significant). □, core (–); ■, core (+).

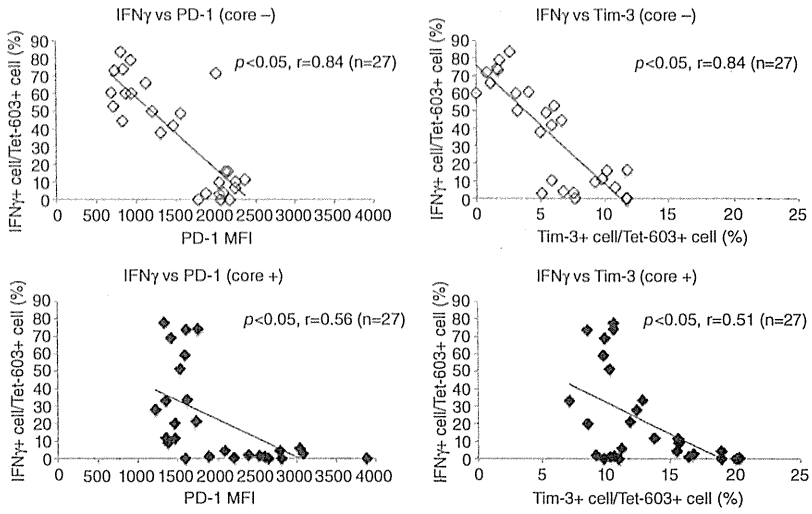

Figure 4 Inverse correlation between the percentages of interferon (IFN)-γ-producing cells and expression of regulatory molecules in antigen-specific intrahepatic CD8 T cells.

When core (+) and core (–) mice were compared, the expression of PD-1 and Tim-3 by Ad-HCV-NS3-specific intrahepatic CD8 T cells was significantly higher in core (+) than core (–) at various time points following Ad-HCV-NS3 infection. Furthermore, we found a significant inverse correlation between the percentages of IFN-γ-producing cells and expression of regulatory molecules in Ag-specific intrahepatic CD8 T cells (Fig. 4).

To determine whether suppression ligand expression by intrahepatic APC is altered in core (+) mice, the intensity of PD-L1 expressed by $CD11^+$ cells was analyzed at 7 and 14 days post-infection. Intrahepatic APC showed the infectious dose-dependent augmentation of PD-L1 expression. We observed elevated expression of PD-L1 by APC in core (+) mice infected with 10^{10} PFU at both time points (Fig. 5a,b). In PD-L1 expression, we did not find a significant difference between Ad-HCV-NS3 infection and Adψ5 control vector infection (Fig. 5c,d).

Taken together, these data suggest that the existence of HCV core gene suppress T-cell-mediated immune response by causing higher expression of suppression molecules.

Ag persistence after Ad-HCV-NS3 infection

To determine the Ag persistence after Ad-HCV-NS3 infection, we analyzed the expression of FLAG-tagged HCV-NS3 protein in the liver by IP-western blot after administration of 2×10^7, 1×10^9 or 1×10^{10} PFU of the virus. The Ag expression in the liver could be found in both core (+) and core (–) mice on 21 days after infection with 1×10^{10} PFU. When 1×10^9 PFU of Ad-HCV-NS3 was administrated, HCV NS3-protein was almost cleared from the liver of core (–) mice at day 21 post-infection, whereas the Ag expression persisted in the liver of core (+) mice until day 21 post-infection (Fig. 6).

It is important to note that the loss of Ag expression in the liver of core (–) mice after infection with 1×10^9 PFU coincided with the high HCV-NS3-specific CD8 T-cell response at 14 days post-infection (Fig. 2c), whereas Ag persistence in the liver of core (+) mice after infection with 1×10^9 PFU or the liver of core (–) and core (+) mice after infection with 1×10^{10} PFU was associated with strongly diminished Ag-specific CD8 T-cell response (Fig. 2c). It is likely that the expression of core protein and the high amount of Ag in the liver contributed to the functional exhaustion of HCV-NS3-specific CD8 T cells.

DISCUSSION

IN THIS STUDY, we found an impaired response of HCV-NS3-specific intrahepatic CD8 T cell in a high dose setting (1×10^{10} PFU) of Ad-HCV-NS3 infection. Furthermore, higher levels of expression of regulatory molecules, Tim-3 and PD-1, by intrahepatic CD8 T cells and PD-L1 by intrahepatic APC were observed in HCV core Tg mice and the expression increased dependent on infectious dose. In addition, we found a significant inverse correlation between the percentages of IFN-γ-producing cells and expression of regulatory molecules

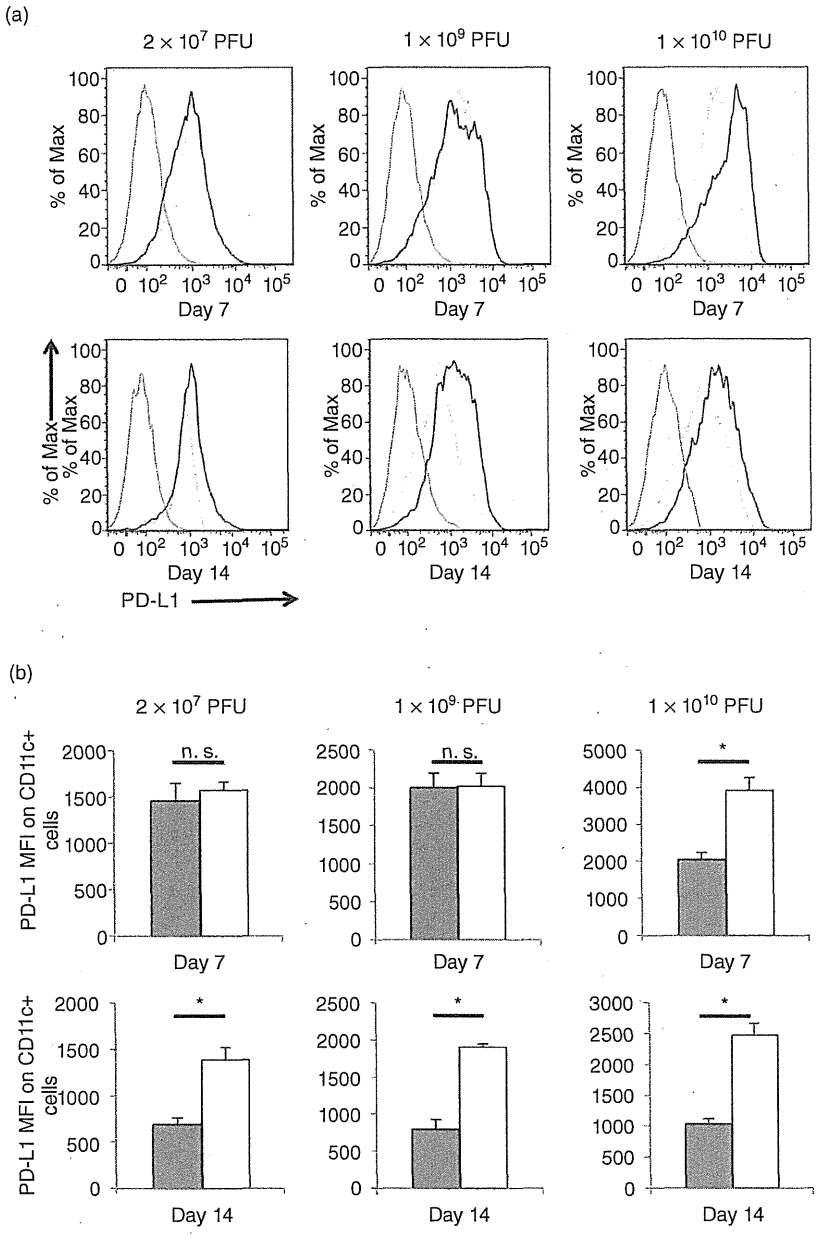

Figure 5 PD-L1 expression in the liver of core (+) and core (−) mice. Core (+) and core (−) mice were injected with 2×10^7, 1×10^9 and 1×10^{10} plaque-forming units (PFU) of adenovirus (Ad)-hepatitis C virus (HCV)-NS3 or Adψ5 control vector. (a) PD-L1 expression by intrahepatic antigen-presenting cells (APC) from core (+) and core (−) mice infected with Ad-HCV-NS3. The % of Max is the number of cells in each sample divided by the number of cells in the sample that contains the largest number of cells. (b) The median fluorescence index (MFI) expression of PD-L1 by intrahepatic $CD11c^+$ leukocyte from core (+) and core (−) mice infected with Ad-HCV-NS3 ($^*P < 0.05$; n.s., not statistically significant). (c) PD-L1 expression by intrahepatic APC from core (+) and core (−) mice infected with Ad-HCV-NS3 or Adψ5 control vector. (d) The MFI expression of PD-L1 by intrahepatic $CD11c^+$ leukocyte from core (+) and core (−) mice infected with Ad-HCV-NS3 or Adψ5 control vector (n.s., not statistically significant). (a) —, isotype; , core (−); —, core (+); (b) ▩, core (−); □, core (+); (c) —, isotype; , Adψ5; —, Ad-NS3; (d) ▩, Adψ5; □, Ad-NS3.

in Ag-specific intrahepatic CD8 T cells. These results indicated that high infectious dose and the presence of HCV core gene were strongly involved in ineffective CD8 T-cell responses.

Recently, a novel mechanism of T-cell dysfunction was demonstrated in a murine model of chronic LCMV infection.[24] It was found that the expression of PD-1 was upregulated on dysfunctional LCMV-specific CD8 T cells in mice.[24] *In vivo* blockade of PD-1/PD-L1 interaction restored the functions of LCMV-specific CD8 T cells and reduced the viral titer.[24] More recently, other inhibitory receptors such as Tim-3 have also been studied as the factors that can cause T-cell impairments in chronic viral infections.[25] These influential discoveries led to

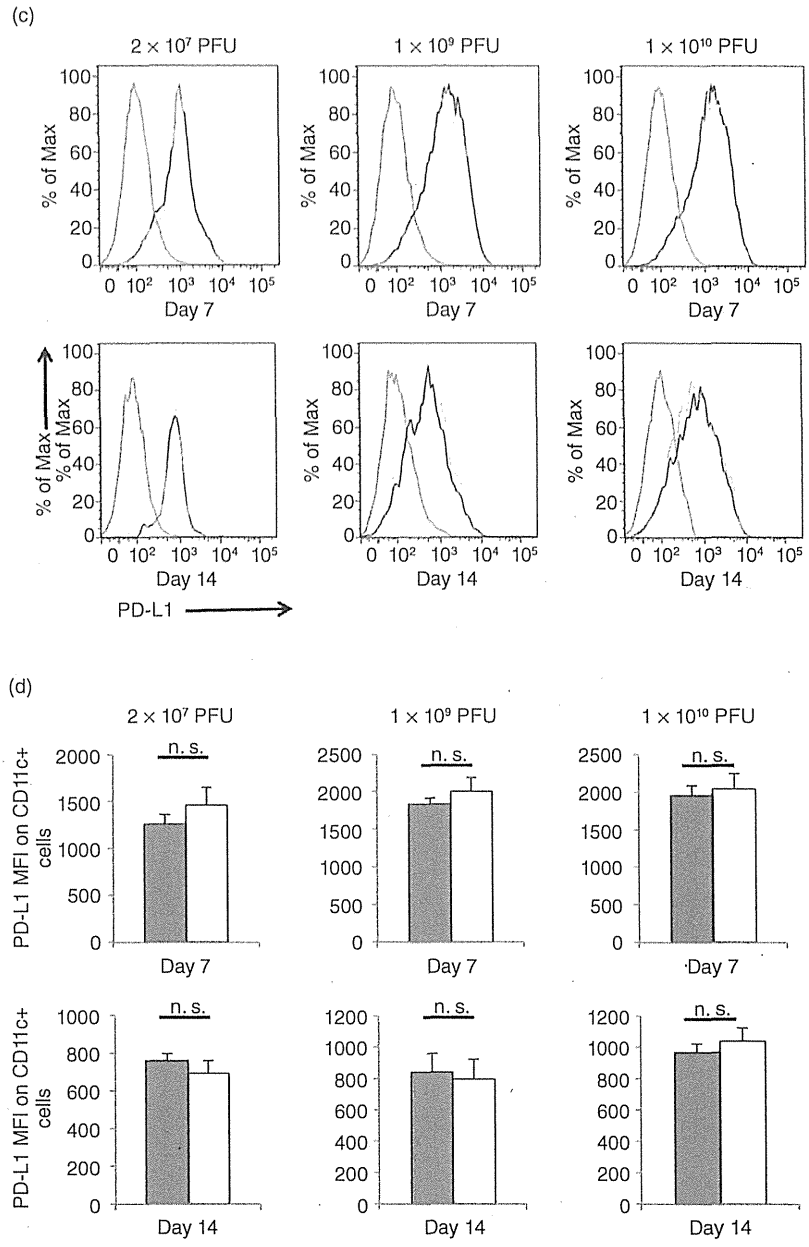

Figure 5 *Continued*

extensive investigations of inhibitory receptors in the regulation of T cells in human chronic viral infections.[25,26]

Chronic HCV infection in humans is characterized by CD8 T-cell exhaustion and dysfunction.[27] As in chronic LCMV infection, the expression of PD-1 is similarly upregulated on the virus-specific CD8 T cells in chronic HCV infection, and HCV-specific PD-1^{high} T cells are functionally impaired.[28–30] Also, Tim-3 is overexpressed on HCV-specific dysfunctional CD8 T cells.[25] In addition, a blockade of PD-1/PD-L1 or Tim-3/galectin9 (Gal9) interaction restores T-cell functions such as proliferation, cytolytic activity and cytokine (IFN-γ and tumor necrosis factor-α) production.[25,28–30] As was

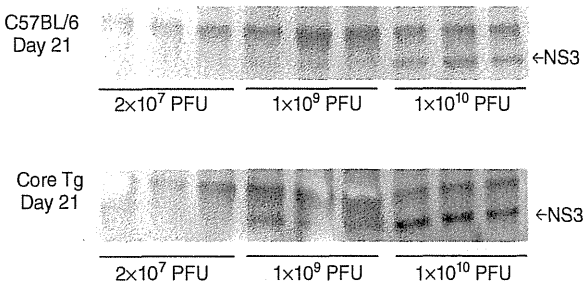

Figure 6 Persisting hepatitis C virus (HCV)-NS3 antigen detection was performed on the liver sections isolated 21 days post-infection. Liver sections were analyzed by IP-western blot assay using anti-FLAG antibody.

mentioned above, it has been reported that increased expression of inhibitory receptors is associated with the impaired HCV-specific CD8 T cells observed in chronic HCV patients. However, the underlying mechanisms for HCV-mediated impaired CD8 T-cell responses have yet to be determined. Based on our finding that lower level of activation and higher levels of expression of regulatory molecules, Tim-3 and PD-1, by intrahepatic CD8 T cells and higher levels of expression of PD-L1 by intrahepatic APC were observed in core (+) mice in comparison with core (−) mice, it is possible that HCV core-induced T-cell dysfunction is one of the viral factors that contributes to impaired CD8 T-cell responses as seen in chronic HCV patients. Our speculation is in accordance with the study by Lukens *et al.*[31]

Suppression of CTL responses via highly expressed Ag was found in chronic HCV infection. Inverse relationships between HCV viral titer and HCV-specific T cells have been reported.[7,32,33] In this study, we found higher levels of expressions of PD-L1 by intrahepatic APC and an impaired intrahepatic CD8 T-cell response in high infectious dose setting. Moreover, we found a significant inverse correlation between the percentages of IFN-γ-producing cells and expression of regulatory molecules in Ag-specific intrahepatic CD8 T cells. It is likely that the PD-1/PD-L1 or Tim-3/Gal9 pathway play a major inhibitory role in our model. High-dose Ad-HCV NS3 infection may inhibit the NS3-specific CD8 T-cell responses not at the induction phase but at the effector phase because Ag-specific-MHC tetramer$^+$ T cells were observed, and most Ag-specific MHC tetramer$^+$ T cells was anergic to PMA/ionophore stimulation and these T cells expressed PD-1 and Tim-3. The role of PD-1/PD-L1 as mechanism for liver tolerance has been well established. PD-1 expression by T cells has been shown to inhibit intrahepatic antiviral immune responses at the effector phase.[34–36]

Hepatitis C virus infection affects approximately 170 million people in the world and is a major global health problem because infected individuals can develop liver cirrhosis and hepatocellular carcinoma. Pegylated interferon and ribavirin therapy, although beneficial in approximately half of treated patients, are expensive and associated with significant side-effects.[37] In this clinical context, there is an urgent need for the development of a therapeutic and/or prophylactic HCV vaccine.[38] Because HCV infects only humans and chimpanzees, it is difficult to evaluate effective therapeutic vaccine candidates. Recently, as a small animal model for HCV infection study, chimeric humanized mouse harboring a human hepatocyte and hematolymphoid system was established by xenotransplantation technique.[39,40] The xenograft model provides a unique opportunity for HCV vaccine development. However, the generation of this chimeric humanized mouse requires advanced technical skills and the scarcity of adequate human primary material remains a significant logistical challenge.[41,42] Our model showed in the present study is easy to create, and it has Ag-specific T-cell exhaustion and Ag persistent in the liver seen in chronic HCV patients. These features suggest that this system is useful for therapeutic HCV vaccine development.

ACKNOWLEDGMENTS

THIS WORK WAS supported by grants from a Saitama Medical University Internal Grant (24-A-1-01 and 24-B-1-06), Grant from Ochiai Memorial Award 2011 and the Ministry of Health, Labor, and Welfare, Japan. The authors thank Hiroe Akatsuka for technical assistance.

REFERENCES

1 Shepard CW, Finelli L, Alter MJ. Global epidemiology of hepatitis C virus infection. *Lancet Infect Dis* 2005; **5**: 558–67.
2 Kamal SM. Acute hepatitis C: a systematic review. *Am J Gastroenterol* 2008; **103**: 1283–97.
3 Alter HJ, Seeff LB. Recovery, persistence, and sequelae in hepatitis C virus infection: a perspective on long-term outcome. *Semin Liver Dis* 2000; **20**: 17–35.
4 Grüner NH, Gerlach TJ, Jung MC *et al.* Association of hepatitis C virus-specific CD8+ T cells with viral clearance in acute hepatitis C. *J Infect Dis* 2000; **181**: 1528–36.

5 Chang KM, Rehermann B, McHutchison JG *et al.* Immunological significance of cytotoxic T lymphocyte epitope variants in subjects chronically infected by the hepatitis C virus. *J Clin Invest* 1997; **100**: 2376–85.
6 Lechmann M, Woitas RP, Langhans B *et al.* Decreased frequency of HCV core-specific peripheral blood mononuclear cells with type 1 cytokine secretion in chronic hepatitis. *Can J Hepatol* 1999; **31**: 971–8.
7 Rehermann B, Chang KM, McHutchison JG *et al.* Differential cytotoxic T-lymphocyte responsiveness to the hepatitis B and C viruses in chronically infected patients. *J Virol* 1996; **70**: 7092–102.
8 Wedemeyer H, He XS, Nascimbeni M *et al.* Impaired effector function of hepatitis C virus specific CD8+ T cells in chronic hepatitis C virus infection. *J Immunol* 2002; **169**: 3447–58.
9 Zinkernagel RM, Hengartner H. Regulation of the immune response by antigen. *Science* 2001; **293**: 251–3.
10 Moskophidis D, Lechner F, Pircher H, Zinkernagel RM. Virus persistence in acutely infected immunocompetent mice by exhaustion of antiviral cytotoxic effector T cells. *Nature* 1993; **362**: 758–61.
11 Wherry EJ, Blattman JN, Murali-Krishna K, van der Most R, Ahmed R. Viral persistence alters CD8 T-cell immunodominance and tissue distribution and results in distinct stages of functional impairment. *J Virol* 2003; **77**: 4911–27.
12 Zajac AJ, Blattman JN, Murali-Krishna K *et al.* Viral immune evasion due to persistence of activated T cells without effector function. *J Exp Med* 1998; **188**: 2205–13.
13 Wherry EJ, McElhaugh MJ, Eisenlohr LC. Generation of CD8 T cell memory in response to low, high, and excessive levels of epitope. *J Immunol* 2002; **168**: 4455–61.
14 Eisen-Vandervelde AL, Waggoner SN, Yao ZQ, Cale EM, Hahn CS, Hahn YS. Hepatitis C virus core selectively suppresses interleukin-12 synthesis in human macrophages by interfering with AP-1 activation. *J Biol Chem* 2004; **279**: 43479–86.
15 Watanabe T, Bertoletti A, Tanoto TA. PD1/PD-L1 pathway and T-cell exhaustion in chronic hepatitis virus infection. *J Viral Hepat* 2010; **17**: 453–8.
16 Yao ZQ, Eisen-Vanderveld A, Waggoner SN, Cale EM, Hahn YS. Direct binding of hepatitis C virus core to gC1qR on CD4+ and CD8+ T cells leads to impaired activation of Lck and Akt. *J Virol* 2004; **78**: 6409–19.
17 Yao ZQ, Nguyen DT, Hiotellis AI, Hahn YS. Hepatitis C virus core protein inhibits human T lymphocyte responses by a complement-dependent regulatory pathway. *J Immunol* 2001; **167**: 5264–72.
18 Cavanaugh VL, Guidotti LG, Chisari FV. Inhibition of hepatitis B virus replication during adenovirus and cytomegalovirus infections in transgenic mice. *J Virol* 1998; **72**: 2630–7.
19 von Freyend MJ, Untergasser A, Arzberger S *et al.* Sequential control of hepatitis B virus in a mouse model of acute, self-resolving hepatitis B. *J Viral Hepat* 2011; **18**: 216–26.
20 Moriya K, Yotsuyanagi H, Shintani Y *et al.* Hepatitis C virus core protein induces hepatic steatosis in transgenic mice. *J Gen Virol* 1997; **78**: 1527–31.
21 Koike K, Moriya K, Ishibashi K *et al.* Sialadenitis histologically resembling Sjogren syndrome in mice transgenic for hepatitis C virus envelope genes. *Proc Natl Acad Sci U S A* 1997; **94**: 233–6.
22 Kolykhalov AA, Agapov EV, Blight KJ, Mihalik K, Feinstone SM, Rice CM. Transmission of hepatitis C by intrahepatic inoculation with transcribed RNA. *Science* 1997; **277**: 570–4.
23 Frelin L, Alheim M, Chen A *et al.* Low dose and gene gun immunization with a hepatitis C virus nonstructural (NS) 3 DNA-based vaccine containing NS4A inhibit NS3/4A-expressing tumors in vivo. *Gene Ther* 2003; **10**: 686–99.
24 Barber DL, Wherry EJ, Masopust D *et al.* Restoring function in exhausted CD8 T cells during chronic viral infection. *Nature* 2006; **439**: 682–7.
25 Golden-Mason L, Palmer BE, Kassam N *et al.* Negative immune regulator Tim-3 is overexpressed on T cells in hepatitis C virus infection and its blockade rescues dysfunctional CD4+ and CD8+ T cells. *J Virol* 2009; **83**: 9122–30.
26 Sharpe AH, Wherry EJ, Ahmed R, Freeman GJ. The function of programmed cell death 1 and its ligands in regulating autoimmunity and infection. *Nat Immunol* 2007; **8**: 239–45.
27 Spangenberg HC, Viazov S, Kersting N *et al.* Intrahepatic CD8+ T-cell failure during chronic hepatitis C virus infection. *Hepatology* 2005; **42**: 828–37.
28 Golden-Manson L, Palmer B, Klarquist J, Mengshol JA, Castelblanco N, Rosen HR. Upreglation of PD-1 expression on circulating and intrahepatic hepatitis C virus-specific CD8+ T cells associated with reversible immune dysfunction. *J Virol* 2007; **81**: 9249–58.
29 Penna A, Pilli M, Zerbini A *et al.* Dysfunction and functional restoration of HCV-specific CD8 responses in chronic hepatitis C virus infection. *Hepatology* 2007; **45**: 588–601.
30 Radziewicz H, Ibegbu CC, Fernandez ML *et al.* Liver-infiltrating lymphocytes in chronic human hepatitis C virus infection display an exhausted phenotype with high levels of PD-1 and low levels of CD127 expression. *J Virol* 2007; **81**: 2545–53.
31 Lukens JR, Cruise MW, Lassen MG, Hahn YS. Blockade of PD-1/B7-H1 interaction restores effector CD8+ T cell responses in a hepatitis C virus core murine model. *J Immunol* 2008; **180**: 4875–84.
32 Sreekumar R, Gonzalez-Koch A, Maor-Kendler Y *et al.* Early identification of recipient with progressive histologic recurrence of hepatitis C after liver transplantation. *Hepatology* 2000; **32**: 1125–30.

33 Sugimoto K, Ikeda F, Standanlick J, Frederick A, Alter HJ, Chang KM. Suppression of HCV-specific T cells without differential hierarchy demonstrated ex vivo in persistent HCV infection. *Hepatology* 2003; **38**: 1437–48.
34 Isogawa M, Furuichi Y, Chisaki FV. Oscillating CD8+ T cell effector functions after antigen recognition in the liver. *Immunity* 2005; **23**: 53–63.
35 Iwai Y, Terawaki S, Ikegawa M, Okazaki T, Honjo T. PD-1 inhibits antiviral immunity at the effector phase in the liver. *J Exp Med* 2003; **198**: 39–50.
36 Maier H, Isogawa M, Freeman GJ, Chisari FV. PD-1:PD-L1 interactions contribute to the functional suppression of virus-specific CD8+ T lymphocytes in the liver. *J Immunol* 2007; **178**: 2714–20.
37 Pawlotsky JM. Therapy of hepatitis C: from empiricism to eradication. *Hepatology* 2006; **43**: S207–20.
38 Callendret B, Walker C. A siege of hepatitis: immune boost for viral hepatitis. *Nature Med* 2011; **17**: 252–3.
39 Legrand N, Ploss A, Balling R *et al.* Humanized mice for modeling human infectious disease: challenges, progress, and outlook. *Cell Host Microb* 2009; **6**: 5–9.
40 Robinet E, Baumert TF. A first step towards a mouse model for hepatitis C virus infection containing a human immune system. *J Hepatol* 2011; **55**: 718–20.
41 Kimura K, Kohara M. An experimental mouse model for hepatitis C virus. *Exp Anim* 2011; **60**: 93–100.
42 Ploss A, Rice CM. Towards a small animal model for hepatitis C. *EMBO Rep* 2009; **10**: 1220–7.

JVI
Journals.ASM.org

Involvement of Hepatitis C Virus NS5A Hyperphosphorylation Mediated by Casein Kinase I-α in Infectious Virus Production

Takahiro Masaki,[a,e] Satoko Matsunaga,[b] Hirotaka Takahashi,[b] Kenji Nakashima,[d] Yayoi Kimura,[c] Masahiko Ito,[d] Mami Matsuda,[a] Asako Murayama,[a] Takanobu Kato,[a] Hisashi Hirano,[c] Yaeta Endo,[b] Stanley M. Lemon,[e,f,g] Takaji Wakita,[a] Tatsuya Sawasaki,[b] Tetsuro Suzuki[d]

Department of Virology II, National Institute of Infectious Diseases, Toyama, Shinjuku-ku, Tokyo, Japan[a]; Proteo-Science Center, Ehime University, Matsuyama, Ehime, Japan[b]; Graduate School of Medical Life Science and Advanced Medical Research Center, Yokohama City University, Fukuura, Kanazawa-ku, Yokohama, Japan[c]; Department of Infectious Diseases, Hamamatsu University School of Medicine, Handayama, Higashi-ku, Hamamatsu, Japan[d]; Lineberger Comprehensive Cancer Center,[e] Division of Infectious Diseases, Department of Medicine,[f] and Department of Microbiology and Immunology,[g] The University of North Carolina at Chapel Hill, Chapel Hill, North Carolina, USA

ABSTRACT

Nonstructural protein 5A (NS5A) of hepatitis C virus (HCV) possesses multiple functions in the viral life cycle. NS5A is a phosphoprotein that exists in hyperphosphorylated and basally phosphorylated forms. Although the phosphorylation status of NS5A is considered to have a significant impact on its function, the mechanistic details regulating NS5A phosphorylation, as well as its exact roles in the HCV life cycle, are still poorly understood. In this study, we screened 404 human protein kinases via *in vitro* binding and phosphorylation assays, followed by RNA interference-mediated gene silencing in an HCV cell culture system. Casein kinase I-α (CKI-α) was identified as an NS5A-associated kinase involved in NS5A hyperphosphorylation and infectious virus production. Subcellular fractionation and immunofluorescence confocal microscopy analyses showed that CKI-α-mediated hyperphosphorylation of NS5A contributes to the recruitment of NS5A to low-density membrane structures around lipid droplets (LDs) and facilitates its interaction with core protein and the viral assembly. Phospho-proteomic analysis of NS5A with or without CKI-α depletion identified peptide fragments that corresponded to the region located within the low-complexity sequence I, which is important for CKI-α-mediated NS5A hyperphosphorylation. This region contains eight serine residues that are highly conserved among HCV isolates, and subsequent mutagenesis analysis demonstrated that serine residues at amino acids 225 and 232 in NS5A (genotype 2a) may be involved in NS5A hyperphosphorylation and hyperphosphorylation-dependent regulation of virion production. These findings provide insight concerning the functional role of NS5A phosphorylation as a regulatory switch that modulates its multiple functions in the HCV life cycle.

IMPORTANCE

Mechanisms regulating NS5A phosphorylation and its exact function in the HCV life cycle have not been clearly defined. By using a high-throughput screening system targeting host protein kinases, we identified CKI-α as an NS5A-associated kinase involved in NS5A hyperphosphorylation and the production of infectious virus. Our results suggest that the impact of CKI-α in the HCV life cycle is more profound on virion assembly than viral replication via mediation of NS5A hyperphosphorylation. CKI-α-dependent hyperphosphorylation of NS5A plays a role in recruiting NS5A to low-density membrane structures around LDs and facilitating its interaction with the core for new virus particle formation. By using proteomic approach, we identified the region within the low-complexity sequence I of NS5A that is involved in NS5A hyperphosphorylation and hyperphosphorylation-dependent regulation of infectious virus production. These findings will provide novel mechanistic insights into the roles of NS5A-associated kinases and NS5A phosphorylation in the HCV life cycle.

Hepatitis C virus (HCV) is a major causative agent of liver-related morbidity and mortality worldwide and represents a global public health problem (1). An estimated 130 million individuals are chronically infected with HCV worldwide, and the treatment of HCV infection imposes a large economic and societal burden (2). HCV is an enveloped virus with a positive-sense, single-stranded RNA genome in the *Hepacivirus* genus within the *Flaviviridae* family (3). The approximately 9.6-kb genome is translated into a single polypeptide of approximately 3,000 amino acids (aa), which is cleaved by cellular and viral proteases to produce the structural proteins (core, E1, E2, and p7) and nonstructural (NS) proteins (NS2, NS3, NS4A, NS4B, NS5A, and NS5B) (4). NS3 to NS5B are sufficient for RNA replication in cell culture (5). NS5B is an RNA-dependent RNA polymerase (RdRp), and NS3 functions as both an RNA helicase and a serine protease (4). NS4A is the cofactor of the NS3 protease, and the NS3-NS4A complex is required for viral precursor processing (4). NS4B induces the formation of a specialized membrane compartment, a sort of membranous web where viral RNA replication may take

Received 30 October 2013 Accepted 14 April 2014
Published ahead of print 23 April 2014
Editor: M. S. Diamond
Address correspondence to Tetsuro Suzuki, tesuzuki@hama-med.ac.jp.
Supplemental material for this article may be found at http://dx.doi.org/10.1128/JVI.03170-13.

doi:10.1128/JVI.03170-13

place (6). NS5A is essential for both viral RNA replication and virion assembly (7–9).

NS5A is an RNA binding protein and exists as a component of the replicase complex (10–13). NS5A is phosphorylated on multiple serine and threonine residues and can be found in hyperphosphorylated (p58) and basally phosphorylated (p56) forms (14–16). Although the distinct mechanisms for generating p56 and p58 forms are still unclear, it has been reported that two regions located around the center and near the C-terminal regions of NS5A are required for basal phosphorylation, while hyperphosphorylation primarily targets serine residues located within low-complexity sequence I (LCS I), which is the linker between domains I and II (15, 17–19). Several phosphorylation sites have been mapped in NS5A by using recombinantly expressed protein and NS5A extracted from cells harboring subgenomic replicons (20–23).

NS5A phosphorylation plays roles in the regulation of viral RNA replication and virion assembly. Some of the cell culture-adaptive mutations in NS4B and NS5A, which reduce NS5A hyperphosphorylation, have been found to confer efficient replication of genotype 1 replicons in Huh-7 cells (17, 18). Similarly, suppression of NS5A hyperphosphorylation through either the use of kinase inhibitors or mutagenesis allows higher RNA replication in non-culture-adapted replicons (18, 24). In contrast, HCV RNA replication is inhibited after treatment of cells carrying adapted replicons with the same kinase inhibitor (24). The C-terminal domain III of NS5A is not essential for viral RNA replication, but it is important for the production of infectious virus. Alanine replacements of the serine cluster in this domain impair NS5A phosphorylation, leading to a decrease in NS5A-core protein interaction, perturbation of the subcellular distribution of NS5A, and disruption of virion production (7–9).

A number of protein kinases have been identified as having the ability to phosphorylate NS5A based on comprehensive screening by using an RNA interference (RNAi) library, recombinantly expressed kinases, and kinase inhibitors (25–28). Among them, casein kinase I-α (CKI-α) and Polo-like kinase 1 (Plk1) have been shown to play roles in viral RNA replication (25, 27). Although silencing of CKI-α inhibits the replication of the genotype 1b subgenomic replicon containing an adaptive mutation (27), its effect on infectious virus production has not been studied to date. Casein kinase II (CKII) has been identified as a positive regulator of virus production via studies with chemical inhibitors and small interfering RNA (siRNA) (9). However, the functional roles of NS5A phosphorylation by its associated kinases in regulation of the viral life cycle are not yet fully understood.

To identify NS5A-associated kinases involved in the HCV life cycle, we developed an *in vitro*, high-throughput screening system for analyzing protein-protein interactions. Using this system followed by *in vitro* phosphorylation assays, we screened human protein kinases on a kinome-wide scale and identified several NS5A-associated kinases. siRNA experiments showed that silencing of CKI-α leads to the most marked inhibition of infectious virus production among the candidate kinases. Here, we report a novel function of CKI-α in the viral life cycle. It is more likely that CKI-α has a more profound impact on virion assembly than on viral replication through hyperphosphorylation of NS5A. Hyperphosphorylated NS5A was predominantly localized in low-density membrane structures around lipid droplets (LDs), in which NS5A interacts with the core for virion assembly, while reduction of NS5A hyperphosphorylation by siRNA targeting CKI-α led to a decrease in NS5A abundance in the low-density membrane structures. The present study provides important insights into the regulatory roles of NS5A-associated kinases and NS5A phosphorylation in the viral life cycle, especially as a molecular switch governing the transition between viral replication and virion assembly.

MATERIALS AND METHODS

Plasmids. Plasmids pJFH1 and pSGR-JFH1/Luc were generated as previously described (29, 30). The JFH-1-based *Gaussia princeps* luciferase (GLuc) reporter construct, which encodes GLuc followed by the foot-and-mouth disease virus (FMDV) 2A protein between p7 and NS2, was generated in a manner similar to the description in a previous report (31). A 1,042-bp double-stranded DNA fragment containing GLuc (32) and FMDV 2A (33) sequences flanked by BsaI and NotI sites at its ends was synthesized and then inserted into the corresponding sites of pJFH1. Related constructs containing serine-to-alanine or serine-to-aspartic acid mutations in NS5A were generated using oligonucleotide-directed mutagenesis techniques. To construct pCAG-CKI-α, the full-length CKI-α-coding sequence was amplified by PCR using cDNAs prepared from Huh-7 cells. The resulting PCR product was then inserted into the multiple-cloning site of pCAGGS (34). pCAG-CKI-α/m6, which contains six silent point mutations that ablate the binding of CKI-α siRNA but maintain the wild-type amino acid sequence of CKI-α, was generated by oligonucleotide-directed mutagenesis of pCAG-CKI-α. All PCR products were confirmed by automated nucleotide sequencing with an ABI Prism 7000 sequence detection system (Life Technologies, Carlsbad, CA).

Cells. The human hepatoma cell line Huh-7, its derivative cell lines Huh7.5.1 (35) (a gift from Francis V. Chisari, The Scripps Research Institute) and Huh7–25 (36), and the human embryonic kidney cell line 293T used to generate HCV pseudoparticles (HCVpp), were maintained in Dulbecco modified Eagle medium (DMEM) supplemented with nonessential amino acids, 100 U of penicillin/ml, 100 μg of streptomycin/ml, and 10% fetal bovine serum (FBS) at 37°C in a 5% CO_2 incubator. SGR-JFH1/LucNeo cells, which harbor a genotype 2a subgenomic replicon carrying a firefly luciferase reporter gene fused to the neomycin phosphotransferase gene of pSGR-JFH1 (37), and LucNeo#2 cells, which harbor a genotype 1b subgenomic replicon carrying a firefly luciferase/neomycin phosphotransferase fusion reporter gene (38, 39) (a gift from Koichi Watashi, National Institute of Infectious Diseases, and Kunitada Shimotohno, National Center for Global Health and Medicine), were cultured in the above medium supplemented with 300 μg/ml G418.

Antibodies. Mouse monoclonal antibody against core protein (2H9) was generated as described previously (30). Anti-NS5A mouse monoclonal antibody (9E10) was a kind gift from Charles M. Rice (The Rockefeller University), and anti-NS5A rabbit polyclonal antibody (TB0705#1) was developed by immunization with the recombinant NS5A protein (8, 40). For detection of cellular proteins, the following antibodies were used: mouse monoclonal antibodies directed against Plk1 (Life Technologies) and glyceraldehyde 3-phosphate dehydrogenase (GAPDH; Millipore, Temecula, CA); rabbit polyclonal antibodies detecting CKI-α (Santa Cruz Biotechnology, Dallas, TX), CKI-ε (Santa Cruz Biotechnology), cyclinc AMP (cAMP)-dependent protein kinase catalytic subunit β (PKACβ; Santa Cruz Biotechnology), phosphatidylinositol 4-kinase IIIα (PI4K-IIIα; Cell Signaling Technology, Danvers, MA), claudin-1 (CLDN1; Life Technologies), calnexin (Enzo Life Sciences, Farmingdale, NY), and GM130 (Sigma-Aldrich, St. Louis, MO); and goat polyclonal antibodies specific for CKII-α′ (Santa Cruz Biotechnology) and apolipoprotein E (ApoE; Millipore). Fluorescence-conjugated secondary antibodies, including Alexa Fluor 488 goat anti-mouse IgG1 and Alexa Fluor 568 goat anti-mouse IgG2a, were purchased from Life Technologies. Horseradish peroxidase (HRP)-conjugated secondary antibodies were from Cell Signaling Technology.

Protein kinase library and cell-free protein synthesis. The construction and identity of the 404 cDNAs encoding human protein kinases used in this study were previously described (41). *In vitro* transcription and cell-free protein synthesis were performed as previously reported (42, 43). Briefly, DNA templates containing a biotin-ligating sequence were amplified by split-primer PCR with kinase cDNAs and corresponding primers and then used for protein synthesis with a fully automated protein synthesizer, a GenDecoder (CellFree Sciences, Ehima, Japan). For synthesis of FLAG-tagged full-length NS5A and domain III proteins derived from the JFH-1 isolate, DNA templates containing a FLAG sequence were generated from the NS5A expression plasmid (8) by split-primer PCR and used with a wheat germ expression kit (CellFree Sciences) according to the manufacturer's instructions.

Amplified luminescent proximity homogeneous assay (AlphaScreen). FLAG-tagged NS5A proteins were mixed with biotinylated kinases in 15 μl of reaction buffer (20 mM Tris-HCl [pH 7.6], 5 mM $MgCl_2$, 1 mM dithiothreitol, and 1 mg/ml bovine serum albumin) in the wells of 384-well OptiPlates (PerkinElmer, Waltham, MA) and incubated at 26°C for 1 h. The mixture was then added to the detection mixture containing 0.1 μl protein A-conjugated acceptor beads (PerkinElmer), 0.1 μl streptavidin-coated donor beads (PerkinElmer), and 5 μg/ml of the anti-FLAG M2 antibody, followed by incubation at 26°C for 1 h. AlphaScreen signals from the mixture were detected using an EnVision device (PerkinElmer) with the AlphaScreen signal detection program.

***In vitro* phosphorylation assay.** To obtain purified kinases used for *in vitro* phosphorylation assays, DNA templates containing a glutathione *S*-transferase (GST)–tobacco etch virus (TEV) sequence were generated by split-primer PCR with kinase cDNAs and corresponding primers and used in a cell-free production system with the wheat germ expression kit as described above. The GST-fusion recombinant proteins were purified on glutathione-Sepharose 4B (GE Healthcare, Buckinghamshire, United Kingdom) and then eluted in 40 μl of phosphate-buffered saline (PBS) containing 5 U of AcTEV protease (Life Technologies) in order to cleave the GST tag from the protein. Biotinylated NS5A proteins were synthesized from DNA templates by using the cell-free BirA system (44). Biotinylated NS5A proteins (40 μl) were coupled on 15 μl of streptavidin Magnesphere Paramagnetics particles (Promega, Madison, WI) and were dephosphorylated by using 10 U of lambda protein phosphatase (New England BioLabs, Ipswich, MA). After washing three times, protein-coupled beads were incubated with 1 μl of purified recombinant kinases at 37°C for 30 min in 15 μl kinase buffer (50 mM Tris-HCl [pH 7.6], 500 mM potassium acetate, 50 mM $MgCl_2$, and 0.5 mM dithiothreitol) containing 1 μCi of [γ-^{32}P]ATP. After the reaction, the beads were washed twice with PBS and then boiled in sample buffer and separated by SDS-PAGE. Phosphorylated NS5A proteins were visualized via autoradiography, and the relative kinase activity of each kinase was determined by normalizing the band intensity of NS5A to that of NS5A incubated with dihydrofolate reductase (DHFR). The band intensities were quantified using Image J software.

Preparation of viral stocks and virus infections. Cell culture-derived infectious HCV particles (HCVcc) were prepared as described previously (30, 36). HCVpp consisting of HCV envelope glycoproteins, the murine leukemia virus Gag-Pol core proteins, and the luciferase transfer vector and pseudoparticles with the vesiclar stomatitis virus G glycoprotein (VSV-Gpp) were generated in accordance with methods described previously (36, 45). Cells seeded onto 24-well plates were transfected with siRNA and/or plasmid DNA as described below and infected with HCVcc for 4 h at a multiplicity of infection (MOI) of 0.5 to 5 or with diluted supernatant containing HCVpp or VSV-Gpp for 3 h. After infection, the cells were washed with PBS and incubated in fresh complete growth medium for 72 h at 37°C until harvest.

siRNA and plasmid DNA transfections. siRNAs were purchased from Sigma-Aldrich. The sequences were as follows: CKI-α, 5′-GGCUAAAGG CUGCAACAAAdTdT-3′ and 5′-UUUGUUGCAGCCUUUAGCCdTdT-3′; CKI-γ1, 5′-GAGAUGAUUUGGAAGCCCUdTdT-3′ and 5′-AGGGC UUCCAAAUCAUCUCdTdT-3′; CKI-γ2, 5′-GCGAGAACUUCCCAGA GGAdTdT-3′ and 5′-UCCUCUGGGAAGUUCUCGCdTdT-3′; CKI-γ3, 5′-CUUACAGGAACAGCUAGAUdTdT-3′ and 5′-AUCUAGCUGU UCCUGUAAGdTdT-3′; CKI-ε, 5′-GCGACUACAACGUGAUGGUdTd T-3′ and 5′-ACCAUCACGUUGUAGUCGCdTdT-3′; CKII-α′, 5′-CCU AGAUCUUCUGGACAAAdTdT-3′ and 5′-UUUGUCCAGAAGAUCU AGGdTdT-3′; PKACβ, 5′-CAAAUAGAGCAUACUUUGAdTdT-3′ and 5′-UCAAAGUAUGCUCUAUUUGdTdT-3′; Plk1, 5′-GUCUCAAGGC CUCCUAAUAdTdT-3′ and 5′-UAUUAGGAGGCCUUGAGACdTdT-3′; TSSK2, 5′-CACCUACUGACUUUGUGGAdTdT-3′ and 5′-UCCAC AAAGUCAGUAGGUGdTdT-3′; ApoE, 5′-GGAGUUGAAGGCCUACA AAdTdT-3′ and 5′-UUUGUAGGCCUUCAACUCCdTdT-3′; CLDN1, 5′-CAGUCAAUGCCAGGUACGAdTdT-3′ and 5′-UCGUACCUGGCA UUGACUGdTdT-3′; PI4K-IIIα, 5′-CCCUAAAGGCGACGAGAGAdTd T-3′ and 5′-UCUCUCGUCGCCUUUAGGGdTdT-3′. The Mission siRNA universal negative control (Sigma-Aldrich), which is designed to have no homology to known gene sequences, was used as a negative control. Silencer Cy3-labeled GAPDH siRNA (Life Technologies) was used to confirm siRNA delivery efficiency. Basically, 10 nM siRNAs were transfected into cells by using Lipofectamine RNAiMax (Life Technologies) according to the manufacturer's recommended procedures. Plk1 siRNA was transfected at 5 nM because of its cytotoxic effect. Plasmid DNA transfection was carried out by using TransIT-LT1 transfection reagent (Mirus, Madison, WI) according to the manufacturer's protocol. For cotransfection of siRNA and plasmid DNA, 6 pmol of siRNA and 200 ng of plasmid DNA were transfected into Huh7.5.1 cells seeded onto a 24-well cell culture plate by using Lipofectamine 2000 (Life Technologies) according to the manufacturer's instructions.

RNA synthesis and electroporation. HCV RNA synthesis and electroporation were basically performed as described previously (8). In the context of coelectroporation of siRNA and an *in vitro*-synthesized subgenomic reporter replicon, or full-length HCV RNA, a total of 3×10^6 to 5×10^6 Huh-7 cells were electroporated with 120 pmol siRNA and 3 μg SGR-JFH1/Luc RNA or 5 μg JFH-1 RNA at 260 V and 950 μF. After electroporation, the cells were immediately transferred onto 24-well or 6-well culture plates or 10-cm cell culture dishes.

Luciferase assay. Cells harboring a subgenomic reporter replicon and HCVpp-infected cells were lysed in passive lysis buffer (Promega). The luciferase activity was determined using a luciferase assay system (Promega) as previously described (46). Secreted GLuc activity was measured in 25-μl aliquots of cell culture supernatants by using the BioLux *Gaussia* luciferase assay kit (New England BioLabs) according to the manufacturer's recommended protocol. The luminescence signal was measured on an Infinite M200 microplate reader (Tecan, Männedorf, Switzerland).

Quantification of HCV core. HCV core protein in cell lysates and culture supernatants was quantified by using a highly sensitive enzyme immunoassay as described previously (8).

RNA extraction and RT-qPCR. Total cellular RNA was extracted with TRIzol reagent (Life Technologies) according to the manufacturer's instructions. Quantification of cellular gene expression was performed by reverse transcription-quantitative PCR (RT-qPCR) using an Applied Biosystems 7500 fast real-time PCR system (Life Technologies) as described previously (47, 48). Primer/probe sets for qPCR targeting CKI-γ1, CKI-γ2, CKI-γ3, and TSSK2 genes were selected from validated Assays-on-Demand products (Life Technologies).

Intra- and extracellular infectivity assays. Intra- and extracellular infectivities of HCVcc were determined as described previously (8). The infectious titers were expressed as focus-forming units (FFU)/ml.

Cell viability assay. Cell viability was determined using the CellTiter-Glo luminescent cell viability assay (Promega) according to the manufacturer's instructions.

Expression of HCV proteins based on vaccinia virus, immunoprecipitation, immunoblotting, and silver staining. HCV protein expression based on vaccinia virus, immunoprecipitation, and immunoblotting were performed as previously described (8). pJFH1 was transfected into

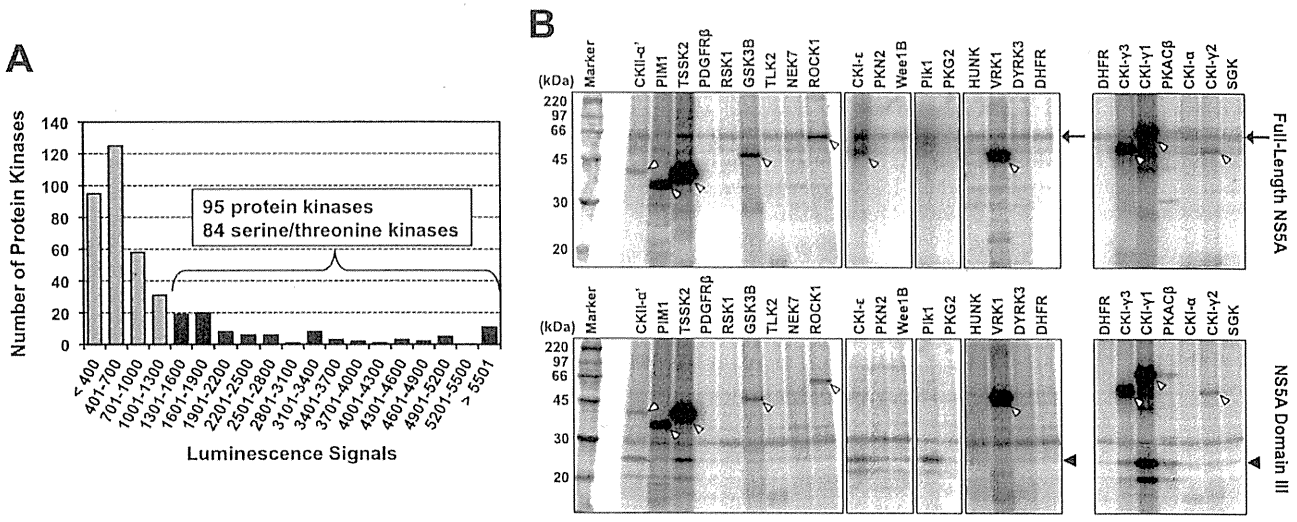

FIG 1 Identification of NS5A-associated kinases. (A) AlphaScreen-based protein-protein interaction assay. FLAG-tagged full-length NS5A, and each of 404 biotinylated human protein kinases, which were synthesized in a cell-free protein production system, were mixed with the detection mixture containing anti-FLAG antibody, protein A-conjugated acceptor beads, and streptavidin-coated donor beads in 384-well plates. Luminescence signals from the mixture were detected. Ninety-five protein kinases were identified with luminescence signals of ≧1,300, of which 84 were serine/threonine kinases. The assay was performed in duplicate for each sample, and data shown are mean values of duplicate experiments. (B) Exemplary autoradiographic images of NS5A phosphorylated *in vitro*. Purified kinases were mixed with biotinylated NS5A proteins coupled on streptavidin beads in kinase buffer containing [γ-^{32}P]ATP. After the reaction, samples were subjected to SDS-PAGE and autoradiography. The arrows, black arrowheads, and white arrowheads indicate phosphorylated full-length NS5A, phosphorylated NS5A domain III, and autophosphorylated kinases, respectively.

cells before infection with vaccinia virus expressing the T7 RNA polymerase. NS5A p58 and p56 protein levels were quantified by densitometry using Image J software. Silver staining of proteins in polyacrylamide gels was carried out using a Silver Stain MS kit (Wako Pure Chemical Industries, Osaka, Japan) in accordance with the manufacturer's protocol.

Subcellular fractionation analysis. Cells were suspended in homogenization buffer (10 mM HEPES-NaOH [pH 7.4], 0.25 M sucrose, and 1 mM EDTA) and disrupted by repeated passages through a 25-gauge needle. After low-speed centrifugation, postnuclear supernatants were layered on linear 11-ml iodixanol gradients from 2.5% to 30% and centrifuged at 40,000 rpm for 3 h in an SW41 rotor (Beckman, Fullerton, CA). Thirteen fractions (0.8 ml in each fraction) were collected from the top of the gradient. Each fraction was concentrated by ultrafiltration units with a 10-kDa molecular mass cutoff (Millipore, Bedford, MA), separated by SDS-PAGE, and immunoblotted with antibodies specific for NS5A, calnexin, and GM130.

Indirect immunofluorescence and microscopy analyses. Cells incubated for 3 days after infection with HCVcc of JFH-1 were fixed with 4% paraformaldehyde for 15 min at room temperature. After washing with PBS, the cells were permeabilized with 0.05% Triton X-100 in PBS for 15 min at room temperature and subsequently incubated in PBS containing 10% goat serum for 1 h. The cells were then costained with antibodies against core and NS5A, followed by incubation with fluorescent secondary antibodies. Cells were counterstained with Hoechst 33342 (Sigma-Aldrich) to label nuclei and BODIPY 493/503 (Life Technologies) to label lipid droplets and then mounted in Vectashield (Vector Laboratories, Burlingame, CA). Subcellular localization of HCV proteins was observed on a Leica SP2 AOBS laser scanning confocal microscope (Leica, Wetzlar, Germany). Colocalization of NS5A and LDs or core was evaluated quantitatively by using the intensity correlation analysis of the Image J software. To statistically compare degrees of colocalization, we determined the intensity correlation quotient (ICQ) (49). ICQ values are distributed between −0.5 and +0.5, with a value of ~0 reflecting random staining and values between 0 and +0.5 versus values between 0 and −0.5 indicative of dependent versus segregated immunolabeling, respectively.

Mass spectrometry analysis. Immunoprecipitated NS5A bands were excised from the gels after silver staining and destained, followed by in gel digestion with trypsin in 50 mM ammonium bicarbonate overnight at 30°C. Liquid chromatography-tandem mass spectrometry (LC-MS/MS) analysis was performed on an LTQ Orbitrap Velos hybrid mass spectrometer (Thermo Fisher Scientific, Bremen, Germany) using Xcalibur (version 2.0.7), coupled to an UltiMate 3000 LC system (Dionex LC Packings, Sunnyvale, CA). The Proteome Discoverer software (version 1.3; Thermo Fisher Scientific) was used to generate peak lists from the raw MS data files. The resulting peak lists were subsequently submitted to a Mascot search engine (version 2.4.1; Matrix Science, London, United Kingdom) and compared against the HCV protein sequences in the NCBI nonredundant protein database (version 20 January 2013; 74,0475 sequences) to identify peptides. The Mascot search parameters were as follows: two missed cleavages permitted in the trypsin digestion; variable modifications including oxidation of methionine, propionamidation of cysteine, and phosphorylation of serine, threonine, and tyrosine; peptide mass tolerance of ±5 ppm; fragment mass tolerance of ±0.5 Da. A minimum Mascot peptide score of 25 was set for peptide selection.

Statistical analyses. Statistical analyses were performed using the Student *t* test unless otherwise noted. A *P* level of <0.05 was considered significant.

RESULTS

A kinome-wide screening of human protein kinases for identification of NS5A-associated kinases. It has been reported that some protein kinases directly or stably associate with HCV NS5A and phosphorylate it *in vitro* (25, 50, 51). To search comprehensively to identify novel NS5A-associated kinases, a kinome-wide screening for interactions of full-length NS5A with human kinases was initially performed. We synthesized 404 human kinases with a wheat germ cell-free protein production system and screened them in terms of their association with NS5A by using a high-throughput assay system based on AlphaScreen technology (Fig. 1A;

TABLE 1 Serine/threonine kinases that exhibited efficient phosphorylation of NS5A

Kinase	LU	Relative kinase activity[a]	
		FL	D3
TSSK2	8,310	4.24	14.94
CKII-α′	5,068	2.30	8.20
Plk1	3,230	2.70	44.65
CKI-γ2	2,602	4.31	3.15
CKI-γ1	2,560	NA	138.69
CKI-γ3	2,218	0.23	52.51
CKI-ε	2,012	7.95	9.48
PKACβ	1,854	0.15	69.54
CKI-α	1,354	4.66	1.00

[a] LU, light units from the AlphaScreen; FL, full-length NS5A; D3, domain III of NS5A. NA, not assessed due to overlap between purified kinases and NS5A on the gel. The relative kinase activity is the fold increase of the *in vitro* activity of each kinase relative to that of DHFR.

see also Table S1 in the supplemental material). Ninety-five proteins were selected as those that possibly bind to NS5A under the cutoff condition of luminescence signals at ≥1,300. Among them, 84 were serine/threonine kinases, and Plk1 and CKII-α′, the catalytic subunit α′ of CKII whose associations with NS5A have been reported (25, 50), were found in the group as signals at 3,230 (Plk1) and 5,068 (CKII-α′). This suggested that our assay system is highly reliable for screening the NS5A-kinase interaction.

In vitro phosphorylation of NS5A by the identified NS5A binding serine/threonine was determined. Each kinase that was synthesized *in vitro* and purified was incubated with either full-length NS5A or domain III of NS5A in the presence of [γ-^{32}P]ATP and separated by SDS-PAGE. Phosphorylated NS5A proteins were then visualized by autoradiography (Fig. 1B). The relative kinase activity was determined by normalizing the band intensity of phosphorylated NS5A with that of NS5A incubated with DHFR, which had no kinase activity and was used as a negative control. Twenty-nine out of 84 serine/threonine kinases were not accurately assessed due to their low levels of expression. As shown in Table 1, among a total of 55 kinases tested (see Table S2 in the supplemental material), nine (CKI-α, CKI-γ1, CKI-γ2, CKI-γ3, CKI-ε, CKII-α′, PKACβ, Plk1, and TSSK2) exhibited efficient phosphorylation of NS5A, defined as a more-than-4-fold or 8-fold increase in activity against the full-length NS5A or domain III of NS5A, respectively, compared to the negative control. Consistent with previous reports (9, 25, 50), Plk1 and CKII-α′ showed apparent kinase activities against NS5A *in vitro*.

Identification of an NS5A-associated kinase, CKI-α, that is important for the HCV life cycle. On the basis of the *in vitro* screenings, nine candidate kinases were further tested as to whether they play roles in the HCV life cycle. We conducted siRNA-based gene silencing of each kinase and assessed its effect on virion production. Huh7.5.1 cells were transfected with siRNAs targeting the kinases and infected with JFH-1 virus at an MOI of 1, 48 h after siRNA transfection. After an additional 72-h incubation, the viral core levels and infectious virus yields in cell culture supernatants were determined. Knockdown efficiencies of the targeted genes at 72 h after JFH-1 infection are shown in Fig. 2A. Efficient knockdown was confirmed either by immunoblotting or RT-qPCR. Figure 2B indicates the effects of gene silencing on virus production (upper panel) and on cell viability by ATP-based luminescence assays (lower panel). An approximately 30-fold reduction in infectious virus yields was observed following knockdown of ApoE, which has been shown to have important roles in HCV assembly and release (52). Among the kinases tested, silencing of CKI-α showed the most profound inhibition of infectious HCV production (~40-fold) without cytotoxicity. Knock down of CKII-α′ and PKACβ led to a moderate reduction in infectious virus pro-

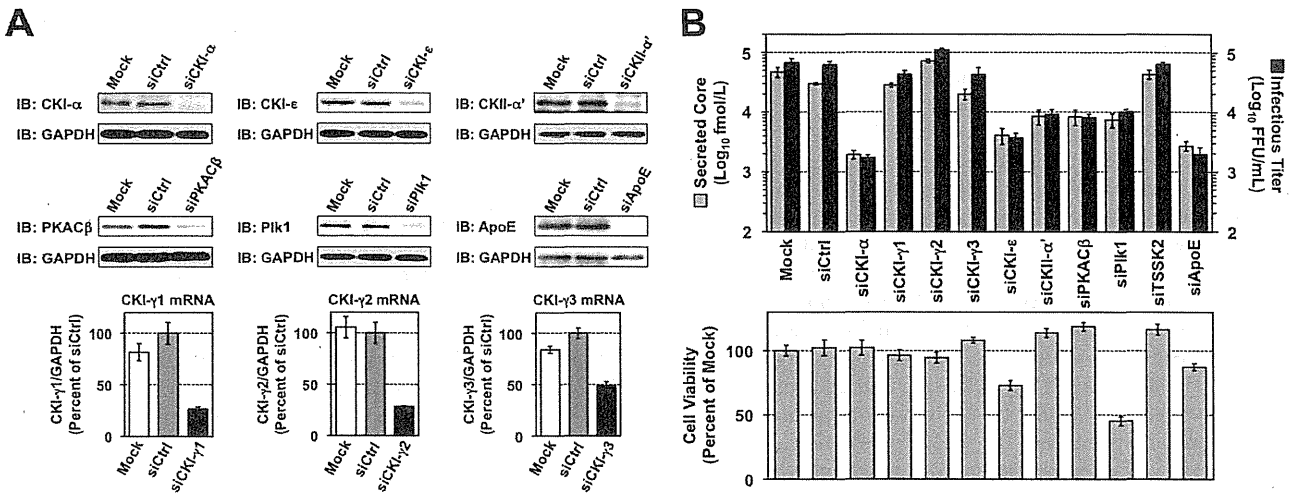

FIG 2 Identification of NS5A-associated kinases involved in the HCV life cycle. (A) siRNA-based gene silencing of NS5A-associated kinases. Huh7.5.1 cells were transfected with siRNAs targeting the indicated genes and were harvested 5 days later for immunoblotting (IB) and RT-qPCR to confirm knockdown efficiencies. mRNA levels of target genes relative to GAPDH mRNA were normalized with values for transfection of control siRNAs (siCtrl), which were set at 100%. Results represent the means ± standard deviations from three independent transfections of siRNA. Mock represents transfection without siRNA. (B) Infectious HCV production and cell viability following knockdown of NS5A-associated kinases. Huh7.5.1 cells were infected with JFH-1 virus at an MOI of 1, 2 days after siRNA transfection. Culture supernatants and cells were harvested 3 days later to determine infectious virus yields (upper panel) and cell viability (lower panel), respectively. Cell viability for each transfection was normalized to that for mock transfection (mock), which was set at 100%. Results shown represent the means ± standard deviations from three independent transfections of siRNA. Mock, transfection without siRNA.

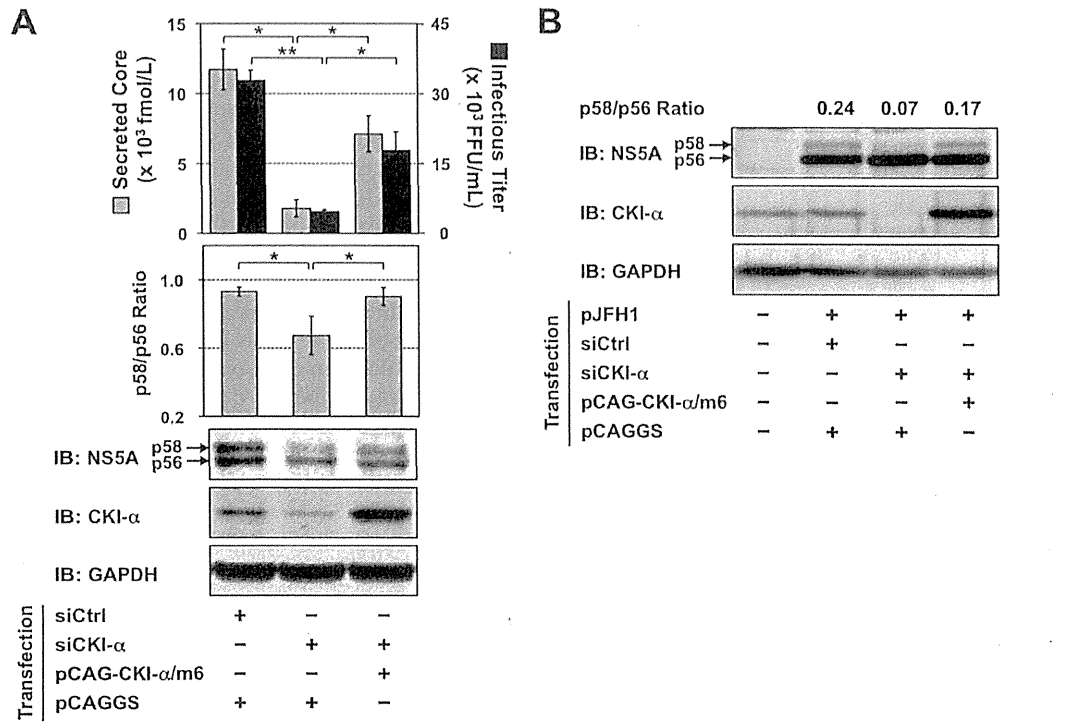

FIG 3 Restoration of NS5A hyperphosphorylation and infectious virus yields by ectopic expression of siRNA-resistant CKI-α. (A) Huh7.5.1 cells were cotransfected with the indicated siRNAs and plasmid DNAs. The next day, cells were infected with JFH-1 virus at an MOI of 0.5. Culture supernatants and cells were harvested an additional 3 days later for measurement of virus yields and immunoblotting (IB). The p58/p56 ratios were calculated after quantifying the band intensities of NS5A. Values shown represent the means ± standard deviations from three replicate experiments. *, $P < 0.05$; **, $P < 0.01$. (B) Huh-7 cells were transfected either with CKI-α siRNA (siCKI-α) or with an irrelevant control siRNA (siCtrl). The next day, cells were retransfected with pJFH1 and pCAG-CKI-α/m6 or empty vector (pCAGGS), followed by infection with vaccinia virus expressing the T7 RNA polymerase at an MOI of 10. NS5A bands were quantified by densitometric analysis, and the p58/p56 ratios were calculated. Immunoblotting images and values shown are representative of two independent experiments.

duction (~10-fold), which was consistent with previous reports showing that CKII-α′ and PKA are involved in virion assembly and viral entry, respectively (9, 53). Knockdown of CKI-ε and Plk1 also resulted in a moderate decrease in virion production (~20-fold), but they induced moderate to severe cell toxicity as well.

Thus, CKI-α, which phosphorylates NS5A, had the highest impact on HCV production based on *in vitro* comprehensive screenings for protein kinases and a subsequent siRNA-based assay.

To further demonstrate that impaired virus production results specifically from CKI-α silencing and is not an off-target effect of the siRNA, cells were cotransfected with CKI-α siRNA and a mutated CKI-α expression vector (pCAG-CKI-α/m6) that contained 6 base mismatches within the site targeted by the CKI-α siRNA without a change in amino acids, followed by JFH-1 infection at an MOI of 0.5 on the next day. The cells and culture supernatants were harvested 3 days later for immunoblotting and titrations of virus yields, respectively (Fig. 3A). Transfection of the CKI-α siRNA led to a significant reduction in infectious virus yields and in the p58/p56 ratio of NS5A. Ectopic expression of the siRNA-resistant CKI-α/m6 apparently restored virus yields ($P < 0.05$), as well as the p58/p56 ratio of NS5A ($P < 0.05$). Similar results regarding the p58/p56 ratio were obtained from immunoblot analysis following vaccinia virus-T7 polymerase-mediated expression of HCV proteins (Fig. 3B). These results indicated that impaired virion production and reduced NS5A hyperphosphorylation are specifically caused by CKI-α silencing. Infectious virus yields showed a closer correlation with the p58/p56 ratio of NS5A than did the expression level of CKI-α, suggesting that the involvement of CKI-α in HCV production is through hyperphosphorylation of NS5A.

CKI-α is mainly involved in virion assembly in the HCV life cycle. Although it has been reported that CKI-α plays roles in the regulation of HCV RNA replication through NS5A phosphorylation, experiments addressing its involvement in the viral life cycle have been performed using the subgenomic replicon system (27). To determine the basic role of CKI-α in the production of infectious HCV, the effect of CKI-α silencing on individual steps in the HCV life cycle was assessed.

First, we used an HCVpp system to analyze viral entry. Two days after the siRNA transfection, the cells were infected with HCVpp derived from JFH-1 or VSV-Gpp and were cultured for a further 3 days (Fig. 4A). Consistent with a previous report (54), CLDN1 knockdown inhibited HCVpp entry by approximately 70%, but not VSV-Gpp entry, compared to transfection with negative control siRNA. CKI-α silencing did not affect HCVpp or VSV-Gpp entry, suggesting that CKI-α is not required for HCV entry.

Second, the effect of CKI-α knockdown was tested using an HCV subgenomic replicon system. Three days after the siRNA transfection, the cells were coelectroporated with the identical siRNA and JFH-1 subgenomic luciferase reporter replicon RNA,